J. Phys. Chem. A **2002,** *106,* 2707−2720

Fundamental Properties and Nature of CH··O Interactions in Crystals on the Basis of Experimental and Theoretical Charge Densities. The Case of 3,4-Bis(dimethylamino)-3-cyclobutene-1,2-dione (DMACB) Crystal

Carlo Gatti,*,† Emanuela May,‡ Riccardo Destro,‡ and Fausto Cargnoni†

CNR-ISTM, Istituto di Scienze e Tecnologie Molecolari, via C. Golgi 19, 20133 Milano, Italy, and Dipartimento di Chimica Fisica ed Elettrochimica, Università degli Studi di Milano, via C. Golgi 19, 20133 Milano, Italy

Received: October 26, 2001; In Final Form: December 18, 2001

The CH··O contacts in the 3,4-bis(dimethylamino)-3-cyclobutene-1,2-dione (DMACB) crystal have been characterized through a topological analysis of its experimental and theoretical densities, derived from a multipole refinement of X-ray diffraction data and from periodic Hartree−Fock calculations, respectively. The existence or the lack of an H··O bond critical point—that is a point through the two nuclei where the gradient of the electron density vanishes—allows us to distinguish between *bonded* and *nonbonded* CH··O contacts, regardless of the value of their H··O separation. The 23 unique bonded contacts in DMACB are characterized by a large and nearly constant (∼140°) C−H−O angle, denoting the importance of the electrostatic energy contribution to such interactions. Instead, the nonbonded ones (four unique for H··O separations up to 3.0 Å) are more bent and may even be folded down to 90°, since their dominant van der Waals contribution to the interaction energy is independent of the C−H−O angle. The CH··O angular distribution observed for H··O separations greater than 2.7 Å is only apparently isotropic, since such isotropy clearly disappears when the bonded and nonbonded contacts are identified and their angular distributions separately analyzed. The Koch and Popelier criteria (*J. Phys. Chem.* **1995**, *99*, 9747) to establish H-bonds are, for the first time, applied in their entirety to a large set of CH··O contacts in a crystalline phase. The criteria are always satisfied by all of the bonded intermolecular CH··O contacts, with a single exception concerning one long bond and one of the six criteria only. The expressions proposed by Espinosa et al. (*Chem. Phys. Lett.* **1998**, *285*, 170), relating the potential energy densities at the critical point to the H-bond strengths, fail when applied to the weak CH··O interactions present in the DMACB crystal. The reasons for such a failure are outlined and new relationships are proposed. The importance of the promolecular charge distributions in defining topological properties of interest to the CH··O bonds is investigated. The criticism raised by Spackman (*Chem. Phys. Lett.* **1999**, *301*, 425) as to the lack of additional information provided by the experimental results to the description of such weak interactions is discussed. It is shown that the promolecular model yields significantly different electron density values at the critical point and in some instances even different topologies, compared to the corresponding multipole or theoretical densities. On the other hand, when the electron density topologies are the same, the values obtained from either electron density for the potential or kinetic energy density at the critical point, are very much alike.

1. Introduction

The most controversial and discussed of the weak hydrogen bond donors in crystals is the C−H group.[1−3] Although CH···O hydrogen bond interactions have been known for more than sixty years,[2,4] they have been widely neglected or their existence even denied,[5] despite conclusive spectroscopic[6] and crystallographic[7] evidence of their structural importance. The scepticism of crystallographers was motivated by the existence in the solid state of stronger hydrogen bonds competing with these weak interactions that, moreover, are comparable in energy with atom−atom van der Waals' interactions.[1] Nowadays, the credibility of CH···O bonding is well assessed[2−4] and thanks in particular to the surge of interest toward statistical database surveys, the characteristics of these interactions have been systematically explored.[1,2,3,8] For example, the role played by CH···O interactions, that is their *function* in Steiner's terms,[2] is now clearly recognized; the CH···O bonds "are important as secondary interactions (···), in determining crystal packing and molecular conformation, in molecular recognition processes, in the stabilization of inclusion complexes, and in the stability and possibly even in the activity of biological macromolecules".[2] Yet, as pointed out by Steiner in his feature paper on CH···O bonds,[2] most of the studies have so far concentrated on the *function* only, not on the *nature* of CH··O hydrogen bonding.

Indeed, the fundamental nature of the CH···O interaction still remains an open and important question. For instance, the lively debate[2,910,11] on the angular preferences, or lack thereof, of the weakest kinds of CH···O interactions is intimately related to their very nature of either directional true hydrogen bonds or of nondirectional van der Waals-like interactions. Among few others,[12−14] two very important studies on the nature of these

---

* To whom correspondence should be addressed. E-mail: c.gatti@istm.cnr.it. Fax: +39 02 50314300.

† CNR-ISTM, Istituto di Scienze e Tecnologie Molecolari.

‡ Dipartimento di Chimica Fisica ed Elettrochimica, Università degli Studi di Milano.

10.1021/jp013980y CCC: $22.00

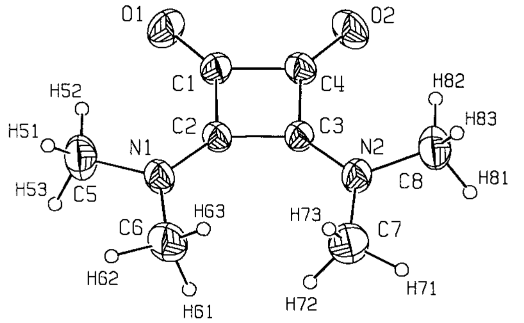

Figure 1. ORTEP drawing showing atomic labels for the DMACB molecule. When reporting their labels throughout the text, the corresponding atoms of the two independent *A* and *B* molecules in the crystal are differentiated by appending an "A" or a "B", respectively, to the atomic labels shown in this figure.

weak H-bonds have been published. A study by Koch and Popelier[15] proposed a characterization of CH··O bonds on the basis of their charge density topology. The other, by Gu, Kar, and Scheiner,[16] convincingly demonstrates that for a series of CH··O bonded molecular complexes of increasing strength, interactions can always be categorized as true H-bonds, rather than as "anti-H bonds",[17] despite the claims that recently appeared in the literature.[18–20] The study by Gu et al.[16] shows that the CH··O interaction behaves very much like a conventional OH···O hydrogen bond in most respects, including equilibrium geometries and sensitivity to deformations from that structure, shifts in electron density that accompany the formation of the bond and, in general, even the relative magnitude of the various components (electrostatic, polarization, charge transfer, dispersion, and exchange) of the interaction energy. Contemporarily, Cubero et al.[14] have shown how the topology of the electron density of C−H···O interactions appears to be essentially the same, regardless of whether the CH bond stretches or contracts, thus confirming the findings of Gu et al.[16]

In this paper, we report a study on the nature of the intramolecular and intermolecular CH···O interactions in the crystal of the DMACB molecule (Figure 1), while in a companion paper,[21] we show how the intermolecular CH···O interactions have an unexpected role, namely to be the cause of the very pronounced enhancement of the molecular dipole when the DMACB molecule crystallizes. In both these studies, the *nature* and *function*[2] of CH···O interactions are derived from an analysis of the experimental and theoretical crystalline electron densities, ρ, rather than from conventional structural approaches.

The main purpose of the present work is to provide an answer to the following questions:

1. Can the true H-bonds, as opposed to van der Waals-like interactions, be unambiguously identified among the CH···O interactions occurring in the DMACB crystal?

2. How large and which are the changes induced on the molecular electron distribution by the formation of the weak intermolecular CH···O bonds?

3. Do any of these changes show up in the promolecule's[22] density?

4. Can a reasonable estimate of the CH··O bond energetics be derived from an analysis of the electron densities only?

It is worth noting that such a comprehensive and deep analysis has never been performed before for the CH···O contacts in a crystalline phase. Moreover, the DMACB crystal represents an excellent candidate for analyzing the characteristics of CH···O interactions in solids, since no other kind of stronger, and thus successfully competing hydrogen bond, is present in the crystal.[23]

The paper is organized as follows. Section 2 gives few details on the crystallographic structure of DMACB crystal and on the experimental and theoretical determination of its electron density, and Section 3 answers the first two of the questions listed above, using the criteria outlined by Koch and Popelier[15] to establish hydrogen bonding. Section 4 explores whether the relationships between topological properties of the electron density and hydrogen bond strengths, proposed by Espinosa et al,[24–26] also apply to the weak CH···O interactions. The role played by the promolecular charge distributions in defining the topological properties of interest to these interactions is then carefully investigated, following an important observation recently formulated by Spackman.[27] Section 5 states the conclusions.

2. Experimental and Computational Details

2.1. Structure of DMACB Crystal. At room temperature, the DMACB molecule crystallizes in the monoclinic $P2_1/n$ space group; at 147 ± 1 K a second-order phase transition from the monoclinic $P2_1/n$ (high T) to the triclinic $P\bar{1}$ (low T) space group was observed.[28] The analysis presented in this paper refers to the low T phase.[29] In the triclinic structure, there are two crystallographically independent types of molecules, hereinafter referred to as *A* and *B* (Figure 2). Each type forms columns of stacked molecules extending along the short axis of the crystal, every molecule in the stack being related to the ones above and below by centers of inversion; the two types of columns (A and B) are quite similar. Each molecule—either *A* or *B*—has eight close neighbors (Figure 2). For a molecule of type *A*, these neighbors are the two adjacent *A* molecules within the column in head-to-tail arrangement, two other type *A* molecules related by translation along the *c* axis, and four *B* molecules in neighboring columns. This molecular arrangement yields several CH···O contacts with H···O distances lying close to or well above the "restrictive"[30] 2.4 Å threshold for potential CH···O hydrogen bonds. Figure 2a and 2b, respectively, show the *inter*- and the *intra*-column CH···O bonded or nonbonded interactions, (see below) which are found for H···O contacts below 3 Å.

2.2. Experimental Electron Density. The experimental electron density of the $P\bar{1}$ phase of the DMACB crystal was derived from the low temperature (20 K) X-ray diffraction study. Details of data collection and multipole refinements will be published elsewhere.[31] Use in the multipole refinement step of the polarized hydrogen atom[32] option in the VALRAY code,[33] enabled us to obtain a final average C−H distance of 1.074 Å. This value is in very close agreement with that determined by neutron diffraction for methyl groups.[34] A similar procedure was recently applied to the structural and electron density determination of a crystal of α-glycine.[35]

A model including quadrupole functions on the H atoms and anisotropic motion for these atoms was used in the analysis of the experimental density, since only this model recovered the intramolecular C−H···O interactions from the charge density topology. The description of thermal motion for H atoms was derived from a rigid-body fit[36] to the anisotropic displacement parameters of the non-H atoms and from infrared spectroscopic information.

Refinement of 817 variables using 12674 observations within $(\sin\theta/\lambda)_{\mathrm{Mo}}^{\mathrm{Max}} = 1.14$ Å^{-1}, gave a final agreement index R_{F} value, and a goodness-of-fit value of 0.0253 and 1.051, respectively.

2.3. Ab Initio Computations. The wave function calculations were performed within the periodic Hartree−Fock (HF) crystalline orbital self-consistent scheme as implemented in the CRYSTAL98[37] suite of programs. For comparison purposes with

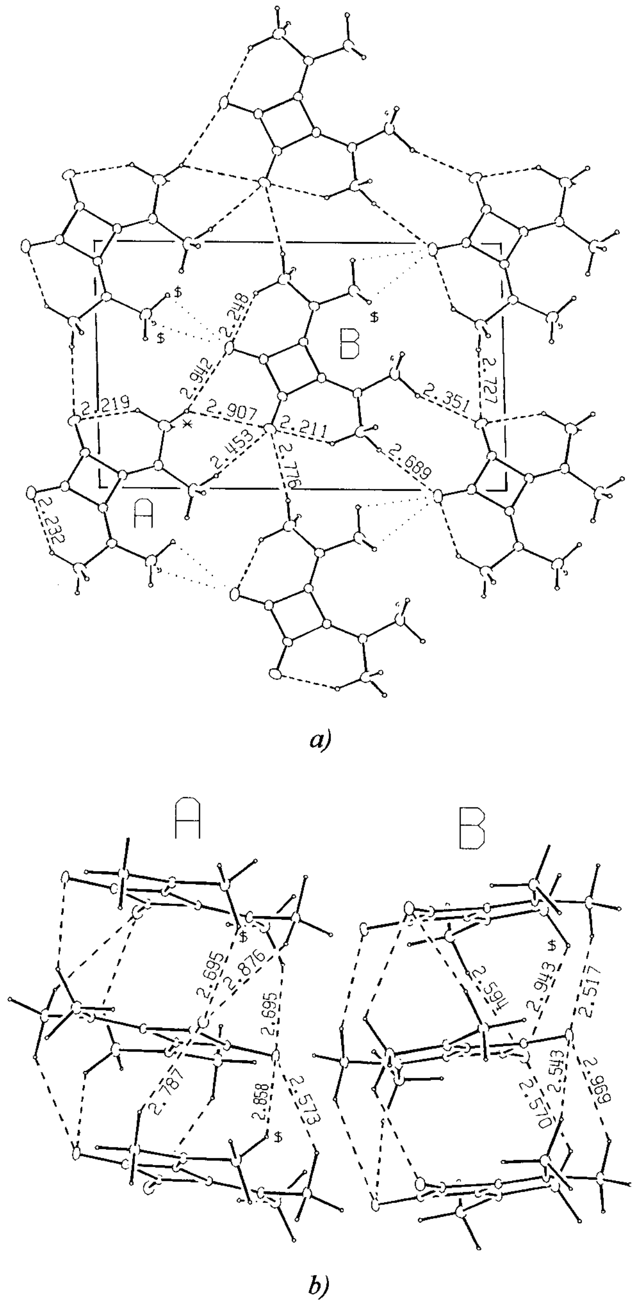

Figure 2. (a) Inter- and (b) intracolumn CH···O interactions in DMACB ($P\bar{1}$ phase) crystals and with H···O distances (reported in Å) below 3.0 Å. There are two crystallographically independent types of molecules, *A* and *B*. Each type forms a column along the short *a* axis of the crystal, every molecule in the column being related to the ones above and below by centers of inversion. The oxygen atoms are involved in six or seven CH··O contacts, some of which are bonded (dashed lines) and some nonbonded (dotted lines) depending on the CHO angle value (see text). The symbol "$" denotes H atoms involved in both bonded and nonbonded contacts, while the symbol "*" marks the H atom forming a bifurcated H-bond.

the crystal calculation, the wave functions for the *A*, *B* molecules and for two *AA′* and *AB* fragments were also evaluated with CRYSTAL98. The latter systems represent computationally convenient fragments for modeling the polymeric network formed by CH···O interactions, and although there are no actual dimers in the crystal structure, they will be referred to as such. *AA′* and *AB* dimers were formed by the closest *AA′* centrosymmetrically related pair and by the two *A*, *B* molecules in the asymmetric unit, respectively. The geometry derived from the low *T* experiment was used for both gas phase and crystal computations. Standard molecular local basis sets (6-21G, 6-31G*)[38] were adopted. Electron densities for the promolecule and for the non interacting molecules in the crystal (procrystal)[22] were obtained with the PATO and MOLSPLIT options of CRYSTAL98, respectively. The size of our system (96 atoms per cell and a single symmetry operation) precluded the use of the more flexible 6-31G* basis set in the evaluation of the atomic properties in the crystal because of the prohibitive computing time required by the atomic boundary determination.[39] Moreover, we were unable to obtain a properly converged 6-31G* wave function for the crystal.[40] The recipe recently suggested by Spackman[41] for overcoming the convergence difficulties encountered in calculations on some molecular crystals with the 6-31G (and 6-31G*) basis sets, if taken alone, was not sufficient in our case. Convergence was only achieved by combining the fulfilment of Spackman's recipe[41,42] with an increase of the scaling factors of the outermost sp shell for all atoms in the molecule to at least 1.08 times their standard molecular values.[43] The ensuing basis set change, however, prevents a proper comparison of crystalline and gas-phase molecular properties with the 6-31G* basis. This should be particularly so for the properties which are sensitive to the local form of the electron density, for instance the location of bond critical points and, as a consequence, of atomic surfaces (see below). The modified 6-31G* basis set was therefore used (for both molecule and crystal calculations) for the interaction energy data only, which were hardly affected by the change of the outermost sp shell contraction factor, while largely dependent on the kind (6-21G or 6-31G*) of basis set adopted. The 6-21G wave functions, while not ensuring very good values for bond and atomic properties on an absolute scale, should be reliable enough for evaluating the changes on such properties induced by crystallization.

The size of our system and the prohibitive computing time for the integrated atomic properties did not allow us to explore the use of basis sets with no $s = p$ constraint for both inner and outer valence functions, as recently encouraged by Spackman[41] for calculations on molecular solids. While the removal of such a constraint results in a smaller basis set superposition error (BSSE)[44] in the estimation of the lattice energy, it also yields CPU times that are much greater than for the case of shared *s* and *p* exponents.[37,45]

2.4. Topological Analysis.

Use of Koch and Popelier[15] criteria to establish hydrogen bonds and use of Espinosa et al.[24,25] relationships for estimating H-bond energetics, required a topological analysis of the electron density performed within the framework of the Quantum Theory of Atoms in Molecules.[46] All the points $\{\mathbf{r}_c\}$ where $\nabla\rho$ vanishes (critical points, CPs) were searched for. Of particular relevance for our analysis were those CPs—named bond critical points (BCPs)—where ρ attains its minimum value (ρ_b) along the atomic interaction lines (AILs). The latter are lines of maximum density with respect to any lateral displacement, defining and isolating the pairwise interactions present in a crystal[47] or in general in an assembly of atoms. Both intra- and intermolecular atomic interactions, settling and characterizing the crystal properties, can be recovered this way. At a BCP—a saddle point in ρ—two of the three eigenvalues or *curvatures* ($\lambda_1 \leq \lambda_2 \leq \lambda_3$) of the Hessian matrix of ρ are negative and the positive (λ_3) curvature is related to an eigenvector directed along the AIL. The properties of the electron density at the BCP (such as the ρ_b value, the values of the curvatures and of their sum equalling the Laplacian of the

TABLE 1: Geometries and Topological Properties of Intermolecular and Intramolecular C−H···O Interactions[a]

O−H	$d_{H\cdots O}$ (Å)	α_{CHO}	$\rho_b \times 100$ theor	$\rho_b \times 100$ expt	$\nabla\rho_b \times 100$ theor	$\nabla\rho_b \times 100$ expt	$\lambda_3 \times 100$ theor	$\lambda_3 \times 100$ expt	$(\lambda_3/\bar{\lambda}_{1,2})^b$ theor	$(\lambda_3/\bar{\lambda}_{1,2})^b$ expt
Intercolumn CH···O Interactions										
O1A−H62B	2.351(7)	159.6(6)	1.13	1.06(13)	5.88	3.61(20)	8.8	6.2	6.3	4.6
O1B−H62A	2.453(8)	142.6(6)	0.84	0.92(10)	4.77	3.09(8)	6.7	5.1	6.7	5.1
O2A−H53B	2.689(8)	124.1(5)	0.54	0.48(7)	3.11	2.29(4)	4.1	3.1	7.5	7.5
O1A−H83A	2.727(8)	119.6(6)	0.46	0.32(9)	2.76	2.04(4)	3.5	2.5	10.0	4.5
O2B−H73A[c]	2.739(8)	97.4(5)	no BCP							
O2A−H72B[c]	2.762(8)	95.1(4)	no BCP							
O2A−H71B[c]	2.781(8)	94.4(5)	no BCP							
O1B−H83B	2.776(8)	119.7(5)	0.41	0.49(6)	2.51	1.98(4)	3.3	2.7	9.4	7.3
O2B−H72A[c]	2.896(7)	89.4(4)	no BCP							
O1B−H53A	2.907(8)	119.3(5)	0.36	0.40(6)	2.09	1.44(4)	2.6	2.0	10.4	7.4
O2B−H53A	2.942(8)	115.7(6)	0.30	0.37(4)	1.87	1.37(2)	2.3	1.8	9.2	8.6
Intracolumn CH···O Interactions (A Molecules)										
O2A−H61A	2.574(7)	136.6(5)	0.66	0.58(9)	3.67	2.51(4)	5.1	3.5	7.3	7.3
O1A−H73A	2.694(8)	132.0(5)	0.48	0.38(7)	2.82	1.95(4)	3.7	2.4	7.4	11.3
O2A−H51A	2.695(7)	130.8(5)	0.59	no BCP	3.08		4.0		10.0	
O1A−H81A	2.787(7)	127.2(5)	0.47	0.27(6)	2.51	1.37(3)	3.1	1.7	10.3	9.3
O2A−H72A	2.858(6)	140.8(5)	0.38	0.51(6)	2.04	1.62(3)	2.5	2.2	10.0	7.8
O1A−H63A	2.875(7)	139.6(5)	0.36	0.37(4)	1.95	1.27(3)	2.4	1.7	10.4	7.5
Intracolumn CH···O Interactions (B Molecules)										
O2B−H61B	2.517(7)	128.4(4)	0.82	0.47(7)	4.34	2.72(4)	6.1	2.9	7.2	11.3
O2B−H51B	2.543(6)	138.1(5)	0.79	0.57(12)	4.15	3.10(8)	5.7	3.9	7.1	9.4
O1B−H73B	2.570(8)	122.6(5)	0.75	0.20(4)	3.95	0.96(3)	5.4	1.2	7.2	9.7
O1B−H81B	2.594(7)	133.9(5)	0.72	0.56(10)	3.74	2.79(8)	5.1	3.4	7.8	11.6
O1B−H72B	2.942(8)	121.9(5)	0.34	no BCP	1.84		2.2		14.6	
O2B−H63B	2.969(8)	120.4(5)	0.32	0.24(3)	1.77	1.12(2)	2.1	1.4	10.5	11.0
Intramolecular CH···O Interactions										
O1A−H52A	2.219(7)	139.2(6)	1.79	1.63(16)	8.36	6.27(25)	13.0	9.5	5.9	5.9
O2A−H82A	2.232(8)	136.6(6)	1.75	1.61(13)	8.17	6.53(21)	12.4	8.7	5.9	7.3
O1B−H52B	2.211(8)	139.0(6)	1.81	1.58(16)	8.45	6.24(25)	13.2	9.4	6.7	5.9
O2B−H82B	2.248(8)	136.3(6)	1.67	1.76(13)	7.95	5.75(17)	11.8	8.4	5.1	6.3

[a] If not otherwise stated, all quantities in au. [b] $\bar{\lambda}_{1,2}$ is the average of the two perpendicular curvatures λ_1 and λ_2. [c] No bond critical point (BCP) present in both the ab initio and experimental densities.

electron density, $\nabla^2\rho_b$) summarize[48] adequately the nature of the associated chemical interaction.

Electron densities $\rho(\mathbf{r})$ were topologically analyzed using the TOPOND98[49] and the PROXRAY[50] packages, for the theoretical and the experimental densities, respectively.

2.5. Atomic Properties. Within the quantum theory of atoms in molecules (QTAM),[46] an atom Ω is defined as the union of a nucleus at $\mathbf{r}_\Omega$ and the associated atomic basin. The latter is a portion of space including the nucleus and enclosed by a surface S defined by the condition $\nabla\boldsymbol{\rho}(\mathbf{r}_s)\cdot\mathbf{n}(\mathbf{r}_s) = 0$, $\mathbf{n}(\mathbf{r}_s)$ being a unit vector normal to the surface at $\mathbf{r}_s$ and $\mathbf{r}_s$ denoting any point of the surface S. Integration of the electron density over the atomic basin of Ω gives the atomic population N_Ω, while the average of the vector $-(\mathbf{r}-\mathbf{r}_\Omega)$ over the electron density in the atomic basin, gives the first moment $\boldsymbol{\mu}_\Omega$ of an atomic electron distribution. The first moments, or atomic dipoles $\boldsymbol{\mu}_\Omega$, arise from the polarization of the atomic electron densities. Atomic populations and first moments were computed for theoretical densities only, using PROMEGA[51] and PROAIMV[52] programs in the case of nonperiodic systems, and TOPOND98[49] code for atoms in the crystal.[53]

3. CH···O Hydrogen Bonds: Geometry, Charge Density Topology, and Charge Density Rearrangements

3.1. CH··O Bond Critical Points Properties. Table 1 lists the intermolecular and intramolecular CH···O contacts present in the DMACB crystal. For the H···O distance ($d_{H\cdots O}$) cutoff, a "long" value of 3.0 Å was selected;[9] this is greater than the van der Waal's sum by 0.3 Å.[54] Bond critical points were found only for those contacts listed in Table 1 that have a C−H−O angle (α_{CHO}) greater than 97.4°.[55] Hereinafter we will term as *bonded* or *non-bonded* those contacts that are, respectively, connected or not connected by an AIL. The bonded contacts span the range 2.211−2.969 Å, with the smaller distances ($2.211 \leq d_{H\cdots O} \leq 2.248$) exhibited by the intramolecular ones. No additional bonded contacts were found by increasing the cutoff for the H···O distance up to 3.5 Å. For both experimental and theoretical densities, the electron density properties at BCPs (Table 1) are typical of closed shell ionic interactions and common to the "conventional" (i.e. not too short) OH···O and NH···O hydrogen bonds.[46,56,57] Charge density is removed from the interatomic surface, resulting in low ρ_b values (*theory*: 0.018−0.003 au), positive $\nabla^2\rho_b$ values (*theory*: 0.084−0.018 au), with small and nearly equal perpendicular curvatures and a comparatively large parallel curvature (λ_3 being typically 1 order of magnitude greater than λ_1 or λ_2). In the case of the experimental densities, the values of ρ_b are at least 3.5 times and, generally, 8−10 times their esd.

3.2. C−H···O Contact Geometry vs CH··O Bond Path Occurrence. The trend of α_{CHO} values vs $d_{H\cdots O}$ distances for the investigated contacts is portrayed in Figure 3. The figure shows that the bonded contacts are moderately bent and have a clear *directional* character, with an α_{CHO} value close to 140° and approximately constant, regardless of the $d_{H\cdots O}$ value. Conversely, the nonbonded contacts are clustered in a very short H···O distances range and characterized by largely bent geometries, the α_{CHO} being close to 90°. Our results for the bonded contacts are in line with a recent structural data survey[9] for CH···O contacts involving, as H-acceptors, organic carbonyl and, as H-donors, the prototypes for C(sp^n)−H groups [ethynyl

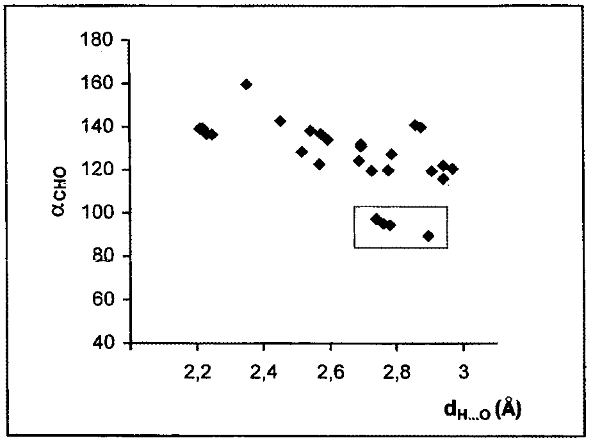

Figure 3. C-H−O angles (α_{CHO}, deg) vs $d_{H\cdots O}$ distances (Å) for CH···O contacts with $d_{H\cdots O}$ below 3 Å; the CH···O contacts that do not exhibit an associated bond path are enclosed in a square box

($n = 1$), vinyl ($n = 2$), and ethyl ($n = 3$)]. This study[9] showed that the angular distribution of CH··O interactions has a clearly recognizable directionality, even for the case of the weakly polarized C(sp^3)−H groups for which a mean α_{CHO} value of 137.1(7) degree was found.[58] However, the CH··O contact directionality observed in the DMACB crystal would not be so neatly manifested if the nonbonded contacts would also be included in the angular distribution analysis. In particular, if this would be the case, one would infer (Figure 3) an almost isotropic CH··O angular distribution for H··O distances larger than 2.7 Å. Instead, the use of the bond path criterion singles out those contacts which presumably are true hydrogen bonds (see below) from those which are better classified as van der Waals' nonbonded contacts. The former are characterized by large α_{CHO} values, because of the important contribution of the monopole-dipole and dipole−dipole interactions favoring linear or close to linear geometries over bent ones, while the latter may also be fold down to $\alpha_{CHO} = 90°$ since their interaction energy is independent of the α_{CHO} value.[9] It is clear that the charge density topology is adding further information to that obtained from the conventional structural analysis. Rather than considering the CH··O contacts beyond $d_{H\cdot\cdot O} = 2.7$ Å as all van der Waals-like,[2,9] we find that:

(a) There are contacts for which the electrostatic contribution is always dominant, even beyond $d_{H\cdot\cdot O} = 2.7$ Å, as demonstrated by the nearly constancy of the C−H−O angle observed for the bonded contacts.

(b) There is no charge accumulation along the van der Waals-like CH··O contacts in DMACB; i.e., regardless of the $d_{H\cdot\cdot O}$ value, the electron density accumulates only along the CH··O interactions dominated by the electrostatic contribution when these are competing with the van der Waals contacts within the same crystal structure.

(c) The cutoff set up by the bond path criterion to establish a CH−O bonded contact appears to be strictly related to the C−H−O angle, rather than to the H···O distance; this result is at odd with the common practice to select the cutoff on the basis of the $d_{H\cdot\cdot O}$ value only.

It is worth noting that the geometrical constraints set forward for the occurrence of CH···O bonded contacts in DMACB crystal agree with the structural patterns previously found in a number of studies of CH···O interactions.[59−61]

Yet, besides the geometrical evidences given earlier and the occurrence of a BCP, how can we prove that the CH··O bonded contacts found in the DMACB crystal are truly H-bonds? The answer is deferred to the following paragraph.

3.3. Fulfillment of Hydrogen Bond Criteria. Koch and Popelier[15] have proposed a set of criteria, based on QTAM, to establish and characterize hydrogen bonds and have shown how they apply not only to H-bonds of a conventional type but also to the rarer, such as the CH··O bonds. These criteria were fulfilled[15] even by bifurcated CH···O hydrogen bonds and have also been applied to characterize hydrogen bonding in CH···π complexes[14] and between opposite charged H atoms.[62] An interesting application of a subset of these criteria to the characterization of various phases of ice has also appeared.[63] However, as of yet they have never been tested in their entirety in crystalline systems. The criteria include (a) the existence of the H-bond critical point and its characteristic topological properties (range of ρ and $\nabla^2\rho$ values); (b) the changes in a number of the H atom integral properties upon H-bonding formation, that is a decrease of its electron population, dipolar polarization and volume, and an increase of its energy; and (c) the mutual penetration of hydrogen and acceptor atoms that accompanies H-bonding. These criteria, with the possible exception of the H volume decrease, were deemed as all *necessary* to conclude that a hydrogen bond is present, while only that related to atomic penetrations has proven, by observation, to be also *sufficient*.[15]

The DMACB molecule and crystal represent excellent candidates for testing the validity of these criteria since the crystal exhibits a large number (23) of unique intra- and intermolecular CH···O bonding interactions. Other features of this system are also of interest. In fact, in the crystal, an H-atom (H53A) is involved in a bifurcated intercolumn H-bond, three other H-atoms (H72A, H73A, H72B) are found to be either bonded or nonbonded to their neighboring oxygen atoms according to the value of the corresponding C−H−O angles, and finally the O-atoms are simultaneously engaged in five (O2A, O2B), six (O1A), or even up to seven (O1B) CH···O bonded interactions.

Tables 2 and 3 display penetrations of H and O atoms, and changes "Δ", (bulk − molecule), in the earlier mentioned H atomic properties upon packing. Data in Tables 2 and 3 refer, respectively, to H atoms involved in intermolecular and intramolecular CH···O interactions. Changes in the O atom populations upon packing are also reported (Table 3). The mutual penetration of H or O atoms upon H-bond formation was estimated by the Δr(X) values (X = H or O, respectively), given as the difference between the bonded, r(X), and the nonbonded, r^0(X), radius of X.[64]

3.3.1. Intermolecular CH···O Interactions. Tables 1 and 2 show that all the criteria proposed by Koch and Popelier are generally very well satisfied by the intermolecular CH···O bonded contacts occurring in the DMACB crystal. Table 2 shows that there are only three outliers, out of a data set of 114 values including four H atomic properties changes and the H and O penetrations for each of the 19 intermolecular H-bonds. The three outliers are the negligible increases (less than 0.9 au), rather than the expected decreases, of the H83A and H83B atomic volumes, and the very small energy stabilization (less than 0.002 au) of H63B atom, instead of the much larger destabilization found for the other H atoms, following H-bond formation.[65,66] If we further consider that, due to a single exception out of a data set of nine H-bonds, the status of a necessary condition to establish H-bond was actually not given[15] to the criterion of the H-atom volume decrease, just one outlier remains in our 114 value data set. In particular, the *sufficient criterion of mutual penetration* of the H and the O acceptor atoms is *clearly fulfilled by all interactions.* Besides, as expected

TABLE 2: Intermolecular CH···O Interactions: Penetrations Δ*r* of Hydrogen and Oxygen Atoms and Δ Changes (Bulk − Molecule) in the Hydrogen Atomic Properties upon Packing[a,b,c]

O---H	$d_{\mathrm{H\cdots O}}$ (Å)	Δ*N*(H)	Δ*r*(H)	Δ*r*(O)	ΔV_{001}(H)	Δ*E*(H)	Δ*μ*(H)
			Intercolumn CH···O Interactions				
O1A−H62B	2.351	−0.067	−0.388	−0.195	−4.1	+0.0271	−0.026
O1B−H62A	2.453	−0.048	−0.328	−0.159	−4.2	+0.0182	−0.021
O2A−H53B	2.689	−0.037	−0.181	−0.079	−2.0	+0.0137	−0.018
O1A−H83A	2.727	−0.035	−0.217	−0.064	*+0.8*	+0.0139	−0.015
O1B−H83B	2.776	−0.020	−0.177	−0.056	*+0.3*	+0.0066	−0.013
O1B−H53A	2.907	−0.024	−0.148	−0.027	−0.4	+0.0078	−0.016
O2B−H53A	2.942	−0.024	−0.122	−0.003	−0.4	+0.0078	−0.016
			Intracolumn CH···O Interactions				
O2B−H61B	2.517	−0.027	−0.342	−0.156	−3.4	+0.0138	−0.016
O2B−H51B	2.543	−0.035	−0.336	−0.173	−4.6	+0.0110	−0.023
O1B−H73B	2.570	−0.028	−0.323	−0.145	−2.3	+0.0107	−0.015
O2A−H61A	2.574	−0.035	−0.307	−0.114	−1.3	+0.0134	−0.019
O1B−H81B	2.594	−0.038	−0.303	−0.150	−4.4	+0.0137	−0.023
O1A−H73A	2.694	−0.046	−0.244	−0.061	−1.4	+0.0180	−0.021
O2A−H51A	2.695	−0.025	−0.240	−0.120	−2.2	+0.0088	−0.017
O1A−H81A	2.787	−0.022	−0.198	−0.071	−0.1	+0.0080	−0.015
O2A−H72A	2.858	−0.021	−0.163	−0.031	−1.8	+0.0069	−0.015
O1A−H63A	2.875	−0.010	−0.147	−0.014	−0.1	+0.0029	−0.012
O1B−H72B	2.942	−0.023	−0.127	−0.010	−1.0	+0.0080	−0.017
O2B−H63B	2.969	−0.002	−0.116	−0.002	−0.3	*−0.0018*	−0.015

[a] If not otherwise stated, all quantities in au. [b] In italics are shown the only values that do not fulfill topological criteria to establish H-bonds (Koch, U.; Popelier, P. L. A. *J. Phys. Chem.* **1995**, *99*, 9747). [c] The V_{001}(H) values refer to the H atomic volumes defined as the region of space enclosed by the intersection of the atomic surface of zero flux and the 0.001 au envelope of $\rho(r)$. The other symbols in Tables 2 and 3, Δ*N*(H), Δ*E*(H), and Δ***μ***(H), are respectively the changes in the H-atom electronic population, electronic energy, and the first moment of its electron distribution.

TABLE 3: Intramolecular CH···O Interactions: Penetrations Δ*r* of Hydrogen and Oxygen Atoms and Δ Changes (Bulk − Molecule) in the Hydrogen and Oxygen Atomic Properties upon Packing[a,b]

O- - -H	$d_{\mathrm{H\cdots O}}$ (Å)	Δ*N*(H)	Δ*N*(O)	Δ*r*(H) (Å)	Δ*r*(O) (Å)	ΔV_{001}(H)	Δ*E*(H)	Δ*μ*(H)
O1A−H52A	2.219	0.033	0.087	0.004	−0.004	2.3	−0.0185	−0.003
O2A−H82A	2.232	0.036	0.087	0.004	−0.004	1.7	−0.0195	−0.004
O1B−H52B	2.211	0.036	0.084	0.006	−0.005	0.4	−0.0200	0.000
O2B−H82B	2.248	0.025	0.082	0.003	−0.004	−0.4	−0.0156	−0.007

[a] If not otherwise stated, all quantities in au. [b] For notation see Table 2.

on the basis of their decreasing H-bond strength, H-atom penetrations are generally found to decrease with the H-bond length increase within each group (intercolumn or intracolumn) of CH···O bonds. Indeed, the H atom (H53A), forming a bifurcated intercolumn H-bond, turns out to be more penetrated ($\Delta r = -0.148$ au) in the direction of the shorter and stronger than it is ($\Delta r = -0.122$ au) along the longer and weaker of the two H-bonds it forms (see also the trend of ρ_b and $\nabla^2\rho_b$ data for these two bonds in Table 1). This general trend is less evidently respected if, rather than considering the H atom penetrations, one examines those of the acceptor oxygen atoms. Hydrogen atoms are also penetrated to a much greater extent than are O atoms, especially for long H-bonds. Larger H-atom penetrations were also found by Koch and Popelier for the CH···O hydrogen bonds in an anti-AIDS compound.[15,67,68]

3.3.2. Intramolecular CH···O Interactions and "Differential" Hydrogen Bond Criteria. Data reported in Table 3 for intramolecular interactions, rather than being changes in atomic properties and atomic penetrations due to H-bond formation, instead represent changes in these quantities with respect to those found for the corresponding H-bonds in the isolated molecule. The changes displayed in Table 3 arise because the O atoms in the crystal are also involved in intermolecular H-bond interactions.

The comparison of intramolecular interactions in gas-phase and crystals provides a test for a "*differential*" application of Koch and Popelier criteria. Namely, the changes in penetrations and in the values of the atomic properties can in principle occur in either direction. That is, an increase or a decrease of each of them may occurr upon crystallization, since the H atoms are already involved in H-bonds in the isolated molecule. One may also presume that if the changes occurring in the bulk for the intramolecular interactions have reverse directions compared to those anticipated by the H-bonding "normal" criteria,[15] then the intramolecular H-bonds will be weakened by the onset of the intermolecular ones. Table 3 shows that this is indeed the case; H atoms involved in the intramolecular CH···O interactions exhibit changes upon formation of the intermolecular CH···O bonds which are opposite to those reported for the remaining H atoms in Table 2.[69] In particular, the changes in electron population and absolute energy values are noticeable and, although reversed, comparable in magnitude to those observed in the formation of intermolecular H-bonds. This is evident in Figure 4 which displays the H atom population changes, Δ*N*(H), as a function of the H··O distance.[70] Table 3 indicates that contrary to the case of H, the O atoms are slightly more penetrated in the bulk, also along the direction of intramolecular CH···O interactions. This opposite behavior with respect to *differential* penetration for the H and their acceptor O atoms is not unexpected. Since the intramolecular H-bond lengths were kept fixed upon change of phase, Δr(H) must be very close to or equal to −Δ*r*(O), provided the bond paths and the BCPs of these H-bonds have not drastically changed their lengths and locations in the bulk. Table 3 shows that while the O atoms are increasing their net charge in the bulk, the H atoms are decreasing it when they are involved in the crystal in intramolecular H-bonds only. The O atoms are found to augment their electron populations because they can withdraw electronic

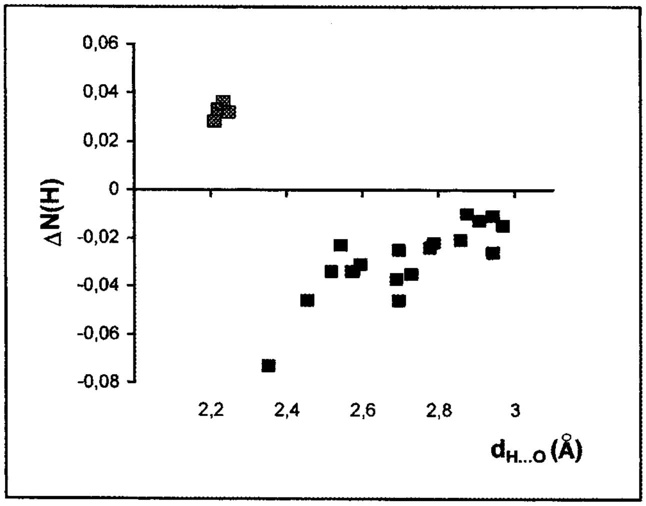

Figure 4. Changes (bulk − molecule) in the H-atom populations N(H) upon packing. Population changes are plotted against the $d_{\mathrm{H}\cdots\mathrm{O}}$ distance of the associated CH···O hydrogen bond(s). H-atoms (gray squares) involved in intramolecular CH··O bonds increase their electron population upon crystallization, the opposite being true for those H-atoms (black squares) that are involved in intermolecular CH··O bonds.

charge from an increased number of H atoms in the bulk. Changes in O-atom populations would therefore suggest an enhanced polarity (and strength) of the intramolecular H-bonds, the reverse being true if the population and the other properties changes of H atoms were considered. In practice, we feel unable to conclude whether the intramolecular H-bonds weaken or strengthen upon formation of the intermolecular ones on the basis of the "*differential*" criteria only.[71] Conversely, changes in the BCP topological properties of such interactions upon crystallization suggest similar H-bond strengths in the two phases, with only a hardly detectable reinforcement of these bonds in the bulk where ρ_b, $\nabla^2\rho_b$, and λ_3 are larger than in the gas phase by less than 1−3%.

4. Interaction Energy, Topology, and Hydrogen Bond Energetics in DMACB Crystal

The experimental charge density is increasingly being used for evaluating the electrostatic contribution to intermolecular interactions.[35,72−77] Electrostatic interactions represent the major contribution to the total interaction energy for crystals containing polar molecules and when such a contribution is supplemented with those deriving from the atom−atom repulsion and dispersive energy terms, a reasonable estimate of the total interaction energy can also be obtained. However, our interest here is more focused on the energies of the individual CH···O interactions and on their energy sum, rather then on the evaluation of the total electrostatic contribution to the packing energy. The latter includes important contributions from the molecular dipole interactions, besides those due to intermolecular CH···O bonds formation.

TABLE 4: Ab Initio Interaction Energies (kJ mol^{-1})

system	IHB[a]	basis set	ΔE[b]	ΔEM[b]
dimer *AA′*	6	6-21G	43.0 (1.7)	21.5 (0.9)
		6-31G*	33.3 (11.5)	16.6 (5.8)
dimer *AB*	3	6-21G	24.6 (9.1)	12.3 (4.5)
		6-31G*	18.0 (11.7)	9.0 (5.9)
crystal	19	6-21G	115.6 (30.3)	57.8 (15.2)
		6-31G*[c]	102.3 (64.6)	51.1 (32.3)

[a] IHB is the number of intermolecular CH··O H-bonds in each system (see Figure 2 and text). The AB pair in the crystal is involved in 38 H-bonds and IHB equals to 19, to avoid double-counting. [b] $\Delta E = -(E_{\mathrm{system}} - E_{\mathrm{molecules}})$, where $E_{\mathrm{molecules}}$ is the energy of the constituent molecules at crystalline geometry and kept at infinite separation one from each other. ΔEM is the interaction energy per DMACB molecule in the system. In parentheses are shown values corrected for BSSE. In the case of the crystal—whose asymmetric unit contains an A−B pair—the ΔEM value is computed with respect to the average of the A and B molecular energies at the crystal geometry. [c] Scale factor for the outermost sp shell: 1.08 (in both molecular and crystal calculations).

Particularly interesting to our scope is the approach relating the charge density to the hydrogen bond dissociation energies, and based on the topological properties of the electron density at the H-bond critical points.[24,25,74] In paragraph 4.2, the application of such an approach to the CH··O interactions in the DMACB crystal is outlined and their resulting bond energies compared to the total ab initio interaction energies discussed in paragraph 4.1. Finally paragraph 4.3 illustrates how the topological properties and related energies of the CH··O interactions compare with those obtained from either the promolecular or the procrystal densities, and using the same topological approach.

4.1. Ab Initio Interaction Energies. Table 4 shows RHF interaction energy Δ*E* data (column 4) for the bulk, the *AA′*, and *AB* dimers, using as gas-phase reference the energy of molecules or pairs evaluated at the crystalline geometry. Listed in columns 2 and 5 are, respectively, the number of intermolecular hydrogen bonds (IHB) in each system and the interaction energies per DMACB molecule (ΔEM). The existence of a bond path (see earlier) was used as a criterion for selecting the CH···O interactions to be included in the evaluation of the IHBs. The AB pair in the crystal is involved in 38 H-bonds and its IHB number amounts to 19, to avoid double counting. Interaction energy data have been corrected for BSSE,[44] using for the bulk the counterpoise procedure, as implemented in CRYSTAL98.[78] Data in Table 4 show that the 6-21G interaction energies are affected by a serious BSSE which seems to be too largely over-corrected by the counterpoise procedure. The 6-31G* estimates appear less affected by BSSE and more reasonably corrected by the adopted counterpoise scheme. This trend in BSSEs nicely agrees with recent findings by Spackman et al.;[41] if we could have adopted a basis set with no $s = p$ constraint for the inner and outer valence shells, we would probably have obtained a further substantial BSSE reduction. The interaction energy per molecule in the crystal is (6-31G* data) about six times larger than in any of the two dimers, as a result of the higher number of IHBs formed in the crystal and of the enhanced electrostatic energy contribution arising from the large induced molecular dipole occurring in the bulk.[21]

4.2. Hydrogen Bond Energetics from Topological Properties. Abramov[79] has recently proposed an approach for the evaluation of the electronic kinetic energy density, *G*(**r**), from the knowledge of the experimental electron density only. This method allows for a quantitative description of the *G*(**r**) behavior at the BCPs of compounds with closed-shell interactions, including H-bonds. By using Abramov's approach and theoretically determined H-bond dissociation energies on a number of bimolecular complexes, Espinosa et al.[24,25] showed that the H-bond energy may be correlated to the electronic potential energy density at the H-bond critical point, $V(\mathbf{r}_b)$. The latter is in turn easily obtained from $G(\mathbf{r}_b)$, using the local statement of the virial theorem[46,80]

$$(h^2/16\pi^2 m)\nabla^2\rho(\mathbf{r}) = 2G(\mathbf{r}) + V(\mathbf{r}) \qquad (1)$$

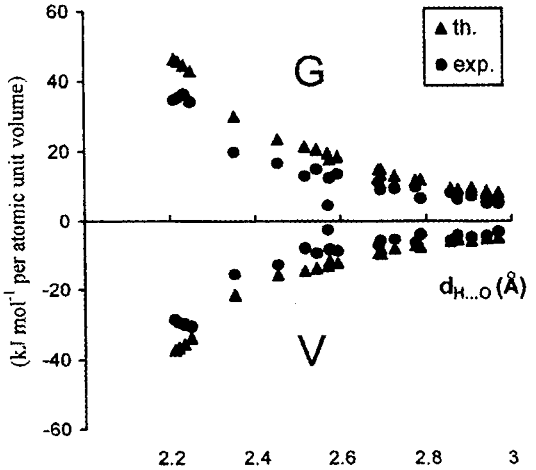

Figure 5. Kinetic, $G(\mathbf{r_b})$, and potential, $V(\mathbf{r_b})$, energy densities (kJ mol^{-1} per atomic unit volume) at the CH··O bond critical point, computed by Abramov's approach.[79] Despite the different and wider $d_{H\cdot\cdot O}$ interval spanned by CH··O bonds in the DMACB crystal, both energy densities depend exponentially on the H···O distance for both experimental and theoretical charge densities as found by Espinosa et al.[24]

TABLE 5: Experimental and Theoretical Kinetic Energy Densities, $G(\mathbf{r_b})$, Local Potential Energy Densities, $V(\mathbf{r_b})$, and Bond Energies, E_{HB} [or $(E_{HB})_{one}$], for CH···O Interactions[a]

	$G(\mathbf{r_b})$		$-V(\mathbf{r_b})$		$-E_{HB}$		
$d_{H\cdots O}$	expt	theor	expt	theor	expt	theor	$-(E_{HB})_{one}$
Intramolecular CH···O Interactions							
2.211	34.8	46.4 (51.7)	28.7	37.3 (47.9)	14.4	18.6	8.8
		45.7 (50.9)		36.9 (47.3)		18.4	
2.219	35.3	45.8 (51.0)	29.4	36.7 (47.0)	14.7	18.4	8.6
		45.4 (50.4)		36.4 (46.5)		18.2	
2.232	36.3	44.6 (49.4)	29.8	35.6 (45.2)	14.9	17.8	8.2
		44.0 (48.7)		35.1 (44.5)		17.5	
2.248	34.1	43.0 (47.5)	30.4	33.8 (42.8)	15.2	16.9	7.7
		42.5 (46.9)		33.5 (42.2)		16.7	
Intermolecular CH···O Interactions							
2.351	19.6	30.0 (31.4)	15.6	21.4 (24.3)	7.8	10.7	5.3
2.453	16.6	23.5 (24.2)	12.9	15.7 (17.1)	6.5	7.8	3.7
2.517	12.9	21.5 (22.1)	7.9	14.5 (15.8)	4.0	7.3	2.9
2.543	14.9	20.5 (21.1)	9.5	13.8 (14.9)	4.8	6.9	2.7
2.570	4.4	19.5 (20.0)	2.6	13.0 (14.0)	1.3	6.5	2.4
2.574	12.4	17.8 (18.1)	8.3	11.5 (12.1)	4.2	5.8	2.4
2.594	13.5	18.4 (18.8)	8.8	12.2 (13.0)	4.4	6.1	2.2
2.689	11.1	14.9 (14.9)	7.1	9.3 (9.4)	3.6	4.7	1.6
2.694	9.2	13.4 (13.4)	5.7	8.2 (8.4)	2.9	4.1	1.6
2.695		14.9 (15.3)		9.6 (10.3)		4.8	1.6
2.727	9.5	13.0 (13.4)	5.5	8.0 (8.7)	2.8	4.0	1.4
2.776	9.7	11.8 (11.9)	6.4	7.1 (7.3)	3.2	3.5	1.2
2.787	6.4	12.0 (12.3)	3.8	7.5 (8.1)	1.9	3.7	1.1
2.858	8.2	9.6 (9.6)	5.8	5.9 (5.8)	2.9	2.9	0.9
2.875	6.2	9.2 (9.1)	4.1	5.5 (5.4)	2.1	2.8	0.8
2.907	7.1	9.8 (9.9)	4.7	5.8 (6.0)	2.4	2.9	0.7
2.942	6.7	8.7 (8.7)	4.3	5.0 (5.1)	2.2	2.5	0.6
2.942		8.6 (8.8)		5.2 (5.6)		2.6	0.6
2.969	5.2	8.3 (8.5)	3.1	4.9 (5.4)	1.6	2.5	0.6

[a] Energy (densities) in kJ mol^{-1} (per atomic unit volume). [a] Values of $G(\mathbf{r_b}\ )$, $V(\mathbf{r_b})$ estimated according to eq 6 of Abramov, Y. A. *Acta Crystallogr.* **1997**, *A53*, 264. E_{HB} estimated according eq 3, $E_{HB} = 1/2V(\mathbf{r_b})$, of Espinosa et al. *Chem. Phys. Lett.* **1998**, *285*, 170, while $(E_{HB})_{one}$ according to $(E_{HB})_{one} = -25.3(6) \times 10^3 \exp(-3.6) d_{H\cdots O}$ of the same reference. For theoretical data, the values in parentheses are the "exact" values, as obtained from the ab initio wave functions. For intramolecular CH···O interactions the second row data refer to gas-phase molecules.

The data set of Espinosa et al.[24,25] included 83 XH···O (X = C, N, O) experimental determinations of H-bonds, 10 of which were CH···O bonds distributed in a much smaller interval of $d_{H\cdot\cdot O}$ distances (2.22−2.59 Å) than that spanned by CH···O bonds in the DMACB crystal. Espinosa et al. found that despite different models, methods, and experimental conditions employed to obtain the BCP topological properties, $G(r_b)$ and $V(\mathbf{r_b})$ depend exponentially on $d_{H\cdot\cdot O}$.

Figure 5 illustrates that our estimates for $G(\mathbf{r_b})$ and $V(\mathbf{r_b})$ also follow an exponential decay vs $d_{H\cdot\cdot O}$, notwithstanding the different and much larger interval of H··O distances. We tested also (Table 5) the application of Abramov's approach and of Espinosa's H-bond energy relationship to our data set. Two estimates[24] of H-bond energies, hereinafter referred to as E_{HB} and $(E_{HB})_{one}$, and derived through Espinosa's relationships, are reported in Table 5.[81] The expression for the latter estimate was obtained by Espinosa et al.[24] from a single-parameter exponential fit (the exponential factor being held fixed) of theoretically determined H-bond dissociation energies vs $d_{H\cdots O}$. The $(E_{HB})_{one}$ estimate is therefore a function of $d_{H\cdots O}$ only. On the other hand, the former estimate, E_{HB}, approximates the H-bond energy (kJ/mol) as $0.5V(\mathbf{r_b})$, where $V(\mathbf{r_b})$ (kJ/mol per atomic unit volume) is obtained through Abramov's approach. It was derived[24] by comparing the exponential fitting curves of $V(\mathbf{r_b})$ and $(E_{HB})_{one}$ vs $d_{H\cdots O}$, the two curves being forced to share a fixed value (−3.6) for the exponential factor.

Table 5 shows that the experimental kinetic energy density at BCP is in most cases about 30% less than its theoretical estimate, as a result of general lower estimates for both ρ_b and $\nabla^2\rho_b$ (see Table 1 above and eq 6 in Abramov's paper[79]). A similar behavior is also exhibited by the potential energy density at BCP, though the lower $\nabla^2\rho_b$ experimental estimates partly compensate for (eq 1) the lower $G(\mathbf{r_b})$ experimental values. As a consequence, the E_{HB} values determined from experiment are about 20% less than those obtained by theory. It is worth noting that the two H-bond energy estimates listed in Table 5 differ considerably in the range of $d_{H\cdot\cdot O}$ distances investigated, E_{HB} being about twice as large as $(E_{HB})_{one}$ for CH···O interactions falling in the distances interval considered by Espinosa[24] and even more so for the longer H···O distances. The discrepancy found at large H··O distances is not surprising since the H-bond energy relationships were fitted to energy and topological data pertaining to shorter CH··O bonds. Less evident is why a significant difference between the two energy estimates still remains in a range of distances that was covered by the analysis of Espinosa.[24] Possible causes include, in the first place, the much larger number of, and the generally shorter H··O distances spanned by the OH··O and NH··O interactions in the Espinosa data set, as compared to the CH··O ones. This lack of balance is likely to result in poorer fits for the CH··O bonds. Second, there was no physical reason to assign a fixed exponential factor to the fitting curves of $V(\mathbf{r_b})$ and $(E_{HB})_{one}$ vs $d_{H\cdots O}$, from which the expression for the E_{HB} estimates was derived.[24] We examine these causes of discrepancy in the following.

The $(E_{HB})_{one}$ energy estimates appear definitely more reasonable than those given by E_{HB}, in view of the general consensus[2] that CH··O energies are typically ≤9.5 kJ mol^{-1} and gradually fade away with increasing separation and decreasing polarization of the C−H bond, reaching a value of about 0.85−1.2 kJ mol^{-1} for the weakest complexes involving nonactivated C−H bonds.[16] The much reliable behavior of the energy estimate depending on the H···O separation only, seems to rule out the possibility to derive reasonable estimates of the CH··O H-bond energies from the charge density topological analysis or at least to adopt, also in this case, the simple $E_{HB} = 0.5V(\mathbf{r_b})$ relationship. To understand why such a relationship seems not to hold at large

TABLE 6: Estimates of Potential Energy Densities, $V(\mathbf{r_b})$, at the H-Bond Critical Points in DMACB from H-Bond Distances: Effect of the Reference Set of H-Bond Interactions Used To Obtain the $V(\mathbf{r_b})$ vs $d_{H\cdot\cdot O}$ Potential Energy Relationships[a,b]

$d_{H\cdots O}$ (Å)	$-V(\mathbf{r_b})_{DMACB,th}$	$-V(\mathbf{r_b})_{DMACB,exp}$	$-V(\mathbf{r_b})_{full,exp}$
	Intramolecular CH···O Interactions		
2.211	34.4 (79)	26.6 (157)	16.9 (88)
2.219	33.7 (78)	26.0 (154)	16.4 (85)
2.232	32.5 (75)	25.1 (149)	15.6 (82)
2.248	31.2 (72)	24.0 (143)	14.8 (77)
	Intermolecular CH···O Interactions		
2.351	23.6 (56)	18.0 (109)	10.1 (55)
2.453	17.9 (43)	13.5 (83)	7.0 (39)
2.517	15.1 (37)	11.3 (70)	5.5 (31)
2.543	14.0 (34)	10.5 (66)	5.0 (28)
2.570	13.1 (32)	9.7 (61)	4.6 (26)
2.574	12.9 (32)	9.6 (61)	4.5 (26)
2.594	12.2 (30)	9.1 (58)	4.2 (24)
2.689	9.5 (24)	7.0 (45)	3.0 (17)
2.694	9.3 (24)	6.9 (44)	2.9 (17)
2.695	9.3 (24)		
2.727	8.5 (22)	6.3 (41)	2.6 (15)
2.776	7.5 (19)	5.5 (36)	2.1 (13)
2.787	7.3 (19)	5.3 (35)	2.1 (12)
2.858	6.0 (16)	4.3 (29)	1.6 (10)
2.875	5.7 (15)	4.1 (28)	1.5 (9)
2.907	5.3 (14)	3.8 (25)	1.3 (8)
2.942	4.8 (13)	3.4 (23)	1.2 (7)
2.942	4.8 (13)		
2.969	4.4 (12)	3.2 (22)	1.1 (7)

[a] $V(\mathbf{r_b})$ estimates as a function of $d_{H\cdot\cdot O}$, given in units of kJ mol^{-1} per atomic unit of volume, were obtained through three different two-parameter exponential fitting curves of $V(\mathbf{r_b})$ vs $d_{H\cdot\cdot O}$. $V(\mathbf{r_b})_{DMACB,yy}$ (yy = th or exp) are obtained from an expression fitting the theoretical (yy = th) or the experimental (yy = exp) DMACB $V(\mathbf{r_b})$ data, while $V(\mathbf{r_b})_{full,exp}$ are obtained from the two-parameter exponential curve of Espinosa et al. (*Chem. Phys. Lett.* **1998**, *285*, 170) fitting 83 experimentally observed XH··O (X = C, N, O) hydrogen bonds. [b] Standard deviations in parentheses.

H···O separations, we made a detailed investigation using the data sets for $V(\mathrm{r_b})$ from our study of the DMACB crystal. The theoretical and experimental $V(\mathbf{r_b})$ data sets[82] of DMACB included 23 and 21 CH··O interactions, respectively, to be compared with the only 10 of such interactions used by Espinosa et al.[24] The two data sets[83] were both fitted with two-parameter unweighted exponential curves, yielding the following expressions for $V(\mathrm{r_b})$ as a function of $d_{H\cdot\cdot O}$:

$$[V(\mathbf{r_b})]_{DMACB,th} = -13.5(24) \times 10^3 \exp[-2.70(6)] d_{H\cdot\cdot O}; \quad r = 0.994 \quad (2)$$

$$[V(\mathbf{r_b})]_{DMACB,exp} = -13.1(59) \times 10^3 \exp[-2.80(17)] d_{H\cdot\cdot O}; \quad r = 0.968 \quad (3)$$

where the subscripts DMACB and yy (yy = th or exp) indicate the $V(\mathbf{r_b})$ data set used to derive eq 2 or 3 and r is the correlation coefficient. Equations 2 and 3 may be compared to the corresponding expression for $[V(\mathbf{r_b})]_{full,exp}$, eq 4, obtained by Espinosa et al.[24] using their "full" $V(\mathbf{r_b})$ data set of 83 experimentally observed H-bonds:

$$[V(\mathbf{r_b})]_{\,full,exp} = -54(18) \times 10^3 \exp[-3.65(18)] d_{H\cdot\cdot O} \quad (4)$$

We use the subscript "full" to remind that eq 4 was derived fitting a data set which includes NH··O and OH··O interactions besides the CH··O ones. Table 6 lists the different $V(\mathbf{r_b})$ estimates obtained from eqs 2−4. Comparison of $[V(\mathbf{r_b})]_{full,exp}$ estimates with the experimental and theoretical $V(\mathbf{r_b})$ data in Table 6 shows that eq 4 largely underestimates $|V(\mathbf{r_b})|$ at all the H-bond critical points in DMACB. This result is not unexpected in view of the general underestimation afforded by eq 4 for the $V(\mathbf{r_b})$ data beyond $d_{H\cdot\cdot O}$ = 2.2 Å. Such an underestimation was pointed out before by Spackman[27] for the strictly related $G(\mathbf{r_b})$ data set and it is also clearly evident from inspection of Figure 1 in ref 24. Table 6 also suggests that the potential energy estimates given by eq 4 and especially eq 3 have a very large uncertainty. By combining eqs 2 through 4 with the two-parameter exponential fit of E_{HB} vs $d_{H\cdot\cdot O}$, eq 5, derived by Espinosa et al using theoretically determined H-bond dissociation energies

$$(E_{HB})_{two} = -a_e \exp[-b_e] d_{H\cdot\cdot O}; \quad a_e = 23(5) \times 10^3;\ b_e = 3.54(10) \quad (5)$$

one obtains relationships for the H-bond energies in terms of $V(\mathbf{r_b})$ and $d_{H\cdot\cdot O}$. They have the general formula given by eq 6:

$$(E_{HB})_{xx,yy} = V(\mathbf{r_b})(a_e/a) \exp[(b - b_e) \mathrm{d}_{H\cdot\cdot O}]; \quad xx = \text{DMACB or full} \quad (6)$$

where b and a are, respectively, the exponential and the multiplier factors (both taken with a positive sign) of eq 2 (yy = th) or of eq 3 (yy = exp). Table 7 lists H-bond energy estimates using eq 6 and compares them with those, $(E_{HB})_{two}$, obtained through eq 5. $(E_{HB})_{DMACB,yy}$ estimates are remarkably similar to $(E_{HB})_{two}$ (Table 7) and to $(E_{HB})_{one}$ (Table 5) for both experimental and theoretical $V(\mathbf{r_b})$ data, while as it is expected the $(E_{HB})_{full,exp}$ estimates are about twice as large. In other words, in the range of large $d_{H\cdot\cdot O}$ distances, the H-bond energies largely deviate from the $0.5V(\mathbf{r_b})$ approximation which would be obtained if one could reasonably equate b_e to b and a_e to $0.5a$ in eq 6. The observed discrepancies between E_{HB} and $(E_{HB})_{one}$ (Table 5) are the result of the following:

(i) The poor $V(\mathbf{r_b})$ estimates at large H··O separations afforded by eq 4 (or by its rather similar one-parameter exponential expression in ref 24).

(ii) The related impossibility to assign a common exponential factor to the fitting curves of $V(\mathbf{r_b})$ and $(E_{HB})_{one}$ in the range of the investigated $d_{H\cdot\cdot O}$ distances. When more suited fittings are used for $V(\mathbf{r_b})$, the H-bond energy expressions given by eq 6 yield very similar results to those given by either $(E_{HB})_{one}$ (Table 5) or $(E_{HB})_{two}$ (Table 7).

The large uncertainties on the fitted H-bond energy estimates derived through eq 6 (even if the DMACB $V(\mathbf{r_b})$ data set is used) and the obvious strong dependence of such estimates on the fitting curve (eq 5) of H-bond energies in terms of the H··O separation, suggest the very limited usefulness of this equation. Conversely, the estimates provided by either $(E_{HB})_{one}$ or $(E_{HB})_{two}$ are remarkably similar and exhibit smaller standard deviations. To conclude, the aim of our analysis was just to explore whether the $(E_{HB})_{one} = {}^{1}/_{2}\mathrm{V}(\mathbf{r_b})$ relationship also applies to the CH··O bonds and, if not, to provide a clear demonstration of why it does not.

Using the $(E_{HB})_{one}$ or $(E_{HB})_{two}$ estimates (Table 5 or 7), the 19 intermolecular CH···O interactions per each A−B pair, yield a significant contribution (34.3 or 36.5 kJ mol^{-1}) to the intermolecular interaction energy in the crystal.[84] This contribution is of the same order of magnitude of the computed total interaction energy (see earlier) and as large as the energy contribution (33.3 or 34.6 kJ mol^{-1}) estimated from the corresponding energy data for the intramolecular CH···O interactions. From $(E_{HB})_{one}$ or $(E_{HB})_{two}$ data, one may also

TABLE 7: Hydrogen Bond Energies (kJ mol^{-1}) of CH···O Interactions in DMACB, from Potential Energy Densities, $V(\mathbf{r_b})$, at the H-Bond Critical Point: Exploring the Effect, on the Estimated Hydrogen Bond Energies, of the Reference $V(\mathbf{r_b})$ Data Set Used To Obtain the H-Bond Energy Relationships[a,b,c]

	$-(E_{HB})_{DMACB,exp}$	$-(E_{HB})_{DMACB,Th}$	$-(E_{HB})_{full,exp}$		
$d_{H\cdots O}$ (Å)	expt	theor	expt	theor	$-(E_{HB})_{two}$
		Intramolecular CH···O Interactions			
2.211	9.9 (65)	9.9 (38)	15.6 (94)	20.3 (123)	9.2 (28)
2.219	10.1 (67)	9.7 (38)	16.0 (97)	20.0 (121)	8.9 (28)
2.232	10.1 (68)	9.3 (36)	16.2 (99)	19.4 (118)	8.5 (27)
2.248	10.2 (68)	8.7 (34)	16.6 (101)	18.4 (113)	8.0 (25)
		Intermolecular CH···O Interactions			
2.351	4.8 (33)	5.1 (20)	8.6 (54)	11.8 (74)	5.6 (1.8)
2.453	3.7 (26)	3.4 (14)	7.2 (46)	8.8 (56)	3.9 (13)
2.517	2.2 (15)	3.0 (12)	4.4 (29)	8.1 (53)	3.1 (10)
2.543	2.6 (18)	2.8 (12)	5.4 (35)	7.8 (51)	2.8 (9)
2.570	0.7 (5)	2.6 (11)	1.5 (10)	7.3 (49)	2.6 (9)
2.574	2.2 (16)	2.3 (9)	4.7 (31)	6.5 (43)	2.5 (9)
2.594	2.3 (16)	2.4 (10)	5.0 (33)	6.9 (46)	2.4 (8)
2.689	1.7 (13)	1.7 (7)	4.1 (28)	5.3 (36)	1.7 (6)
2.694	1.4 (10)	1.5 (6)	3.3 (22)	4.7 (32)	1.7 (6)
2.695		1.7 (7)		5.5 (38)	1.7 (6)
2.727	1.3 (10)	1.4 (6)	3.2 (22)	4.6 (32)	1.5 (5)
2.776	1.5 (11)	1.2 (5)	3.7 (26)	4.1 (29)	1.2 (4)
2.787	0.9 (6)	1.2 (5)	2.2 (15)	4.3 (30)	1.2 (4)
2.858	1.2 (9)	0.9 (4)	3.4 (24)	3.4 (24)	0.9 (3)
2.875	0.9 (6)	0.8 (4)	2.4 (17)	3.2 (23)	0.9 (3)
2.907	1.0 (7)	0.9 (4)	2.8 (20)	3.4 (24)	0.8 (3)
2.942	0.9 (6)	0.7 (3)	2.5 (18)	2.9 (21)	0.7 (3)
2.942		0.8 (3)		3.1 (22)	0.7 (3)
2.969	0.6 (5)	0.7 (3)	1.8 (13)	2.9 (21)	0.6 (2)

[a] $(E_{HB})_{XX,YY}$ estimates obtained from eq 6 (see text). These expressions were obtained by combining fitting curves for $V(\mathbf{r_b})$ data vs $d_{H\cdots O}$ and the two-parameter exponential expression for H-bond energy vs $d_{H\cdots O}$, $-(E_{HB})_{two} = 23(5) \times 10^3 \exp(-3.54(10)d_{H\cdots O})$, derived by Espinosa et al. (*Chem.Phys. Lett.* **1998**, *285*, 170) using ab initio dissociation energies of H-bonded model systems. The *xx* (*xx* = DMACB or full) and *yy* (*yy* = exp or th) refers to the $V(\mathbf{r_b})$ data set used to obtain the fitting curve for $V(\mathbf{r_b})$ data vs $d_{H\cdots O}$ (see Table 6). Values of $(E_{HB})_{two}$ are reported for the sake of comparison with the H-bond energy estimates in terms of $V(\mathbf{r_b})$ and $d_{H\cdots O}$ data. [b] H-bond energy values obtained from experimental or theoretical DMACB $V(\mathbf{r_b})$ data are labeled in the table by "exp" and "th", respectively. [c] H-bond energies standard deviations, computed on the basis of the standard deviations for the fitting parameters, are reported in parentheses.

estimate the energy contribution due to CH···O intermolecular interactions in the *AA′* (six H-bonds, with $d_{H\cdot\cdot O}$ distances equal to 2.694, 2.695, and 2.876 Å, Figure 2) and *AB* dimer (three H-bonds, with $d_{H\cdot\cdot O}$ distances equal to 2.453, 2.907, and 2.942 Å). They are, respectively, 8 and 10 kJ mol^{-1}, using $(E_{HB})_{one}$ estimates. Both values are comparable to the ab initio interaction energies for the corresponding dimers, provided that the larger 6-31G* basis is adopted and the BSSE correction is applied (see Table 4).

Table 5 also confirms that the strength of the intramolecular CH···O bonds is hardly affected by crystallization, the corresponding E_{HB} values increasing by less than 0.3 kJ mol^{-1} in the bulk.

For the sake of comparison with the corresponding Abramov's estimates, also reported in Table 5 are the "exact" theoretical values for $G(\mathbf{r_b})$ and $V(\mathbf{r_b})$. Abramov's approach is found to perform successfully for this kind of interaction and range of H···O distances. The differences between "exact" $G(\mathbf{r_b})$ values and their estimates never exceed 10% in the case of the intramolecular CH···O interactions and the discrepancies are even smaller (∼2−3%) for the intermolecular ones. Thus, the agreement is further improving as the H··O distance increases.

In his paper, Abramov[79] pointed out that a proper comparison between $G(r_b)$ estimates from experiment and theory should include an adequate treatment of the effects of the crystal field and of the intermolecular interactions in the evaluation of the theoretical $G(\mathbf{r_b})$ also. To the best of our knowledge, data in Table 5 provide the first example where such a proper comparison takes place.

4.3. Effects of the Deformation and Interaction Densities on the Topological Properties at the CH··O Bond Critical Points. It has been recently shown by Spackman[27] that the "essential behavior exhibited by multipolar refined electron densities for X−H··O contacts can be described remarkably well by the superposition of realistic spherical electron densities for O and H atoms and the separation between them". In particular it was demonstrated[27] that a simple two-atom model accounts for the observed exponential dependence of both $G(\mathbf{r_b})$ and $V(\mathbf{r_b})$ on the H···O distance. This result prompted Spackman to raise the important question of "whether present experimental results differ from a simple reference model, that is the promolecular density, for weak interactions".[27] To gain a further insight on this important observation, we first investigated how close the properties of the promolecule and of the crystal density is in a case that is unaffected by systematic experimental errors. Figure 6a shows the dependence of $G(\mathbf{r_b})$ and $V(\mathbf{r_b})$ values on the H···O distance for the 6-21G crystal density and for the promolecular density obtained with the same basis set. $G(\mathbf{r_b})$ data correspond to the exact values as they were not approximated through Abramov's expression in this case. The two electron densities behave similarly for both $G(\mathbf{r_b})$ and $V(\mathbf{r_b})$. These energy densities also show a clear and similar exponential dependence on the H···O distance for either of the two electron densities. However, a close inspection of Figure 6a reveals that the promolecular curve of $V(\mathbf{r_b})$ or $G(\mathbf{r_b})$ crosses the crystal density curve at $d_{H\cdot\cdot O}$ distances equal to about 2.3−2.4 Å. The two energy densities are both smaller in magnitude at short $d_{H\cdot\cdot O}$ distances for the promolecular density, the opposite being true beyond 2.4 Å. A curve crossing is also observed (Figure 6b) for $\nabla^2\rho_b$ data, the crystal density values being bigger at short and smaller at large $d_{H\cdot\cdot O}$ distances. Instead, greater ρ_b values are found (Figure 6c) at any $d_{H\cdot\cdot O}$ distance for the promolecular density. The curve crossing for *G* (and *V*) data mentioned above is easily rationalized in terms of the observed crossing for $\nabla^2\rho_b$

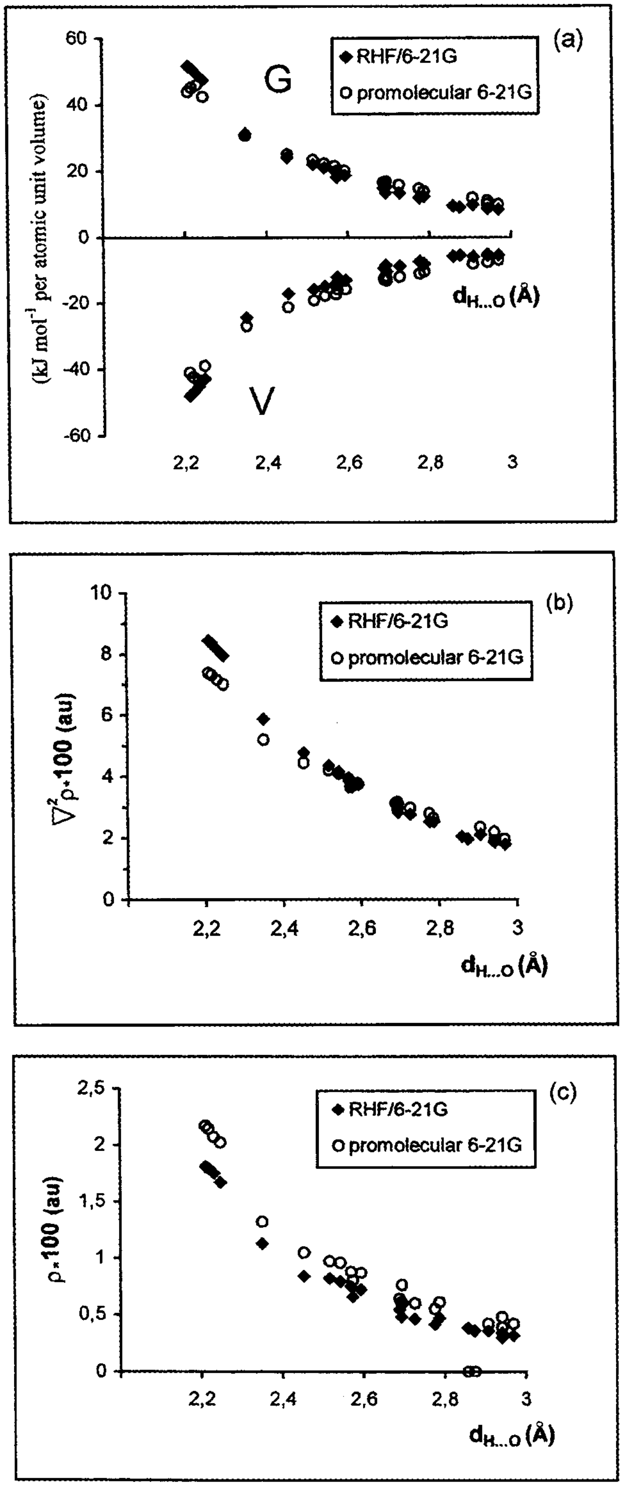

Figure 6. Topological properties at the CH··O bond critical point, for the RHF/6-21G crystal density and for the 6-21G promolecular density: (a) Kinetic, $G(\mathbf{r}_b)$, and potential, $V(\mathbf{r}_b)$, energy densities (kJ mol^{-1} per atomic unit volume). The $G(\mathbf{r}_b)$ values are "exact" and were not approximated through Abramov's approach.[79] (b) Electron density Laplacian $\nabla^2\rho_b$ and (c) electron density ρ_b. In the case of the promolecular density, a value of $\rho_b = 0$ is conventionally assigned to the CH··O interactions which do not have a bond critical point.

data. As pointed out by Spackman,[27] a close inspection of the relative contributions of $\nabla^2\rho_b$ and ρ_b to $G(\mathbf{r}_b)$ shows that ρ_b dominates at small distances, but the contribution from $\nabla^2\rho_b$ increases with separation while that from ρ_b decreases, until for $d_{H\cdot\cdot O} > 2.5$ Å $\nabla^2\rho_b$ contributes >80% of the value of $G(\mathbf{r}_b)$.[85]

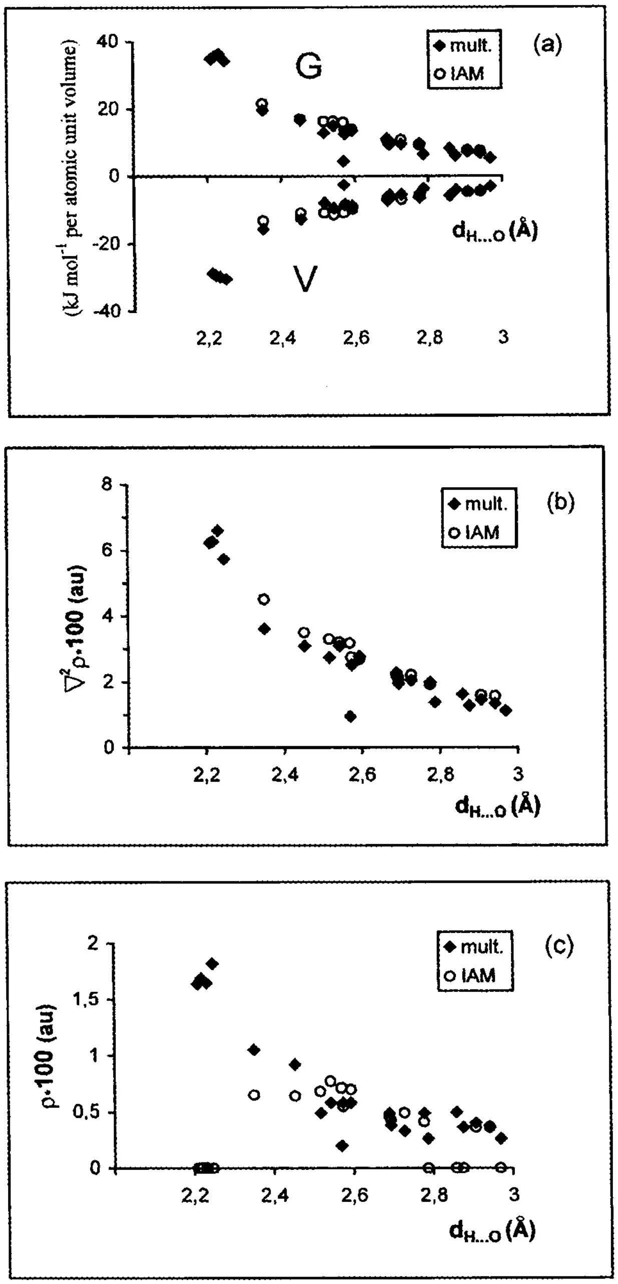

Figure 7. Topological properties at the CH··O bond critical point, for the experimental and IAM densities: (a) Kinetic, $G(\mathbf{r}_b)$, and potential, $V(\mathbf{r}_b)$, energy densities (kJ mol^{-1} per atomic unit volume). The $G(\mathbf{r}_b)$ values were evaluated through Abramov's approach.[79] (b) Electron density Laplacian $\nabla^2\rho_b$ and (c) electron density ρ_b. In the case of the IAM density, a value of $\rho_b = 0$ is conventionally assigned to the CH··O interactions which do not have a bond critical point.

Therefore, the larger $\nabla^2\rho_b$ values found for the promolecular density at separations >2.5 Å yield greater $G(\mathbf{r}_b)$ and $|V(\mathbf{r}_b)|$ (see eq 1) values for this model density beyond 2.3−2.4 Å.

When the experimental crystal density of DMACB is compared (Figure 7) to that given by the independent atom model (IAM), the following important observations can be made:

(i) No bond critical point is found (Figure 7c) in the promolecular (IAM) density for the four intramolecular CH··O interactions and for four of the 19 CH··O intermolecular bonds. Therefore, the IAM density differs from the experimental density in important topological features that are related to the H-bonding network. Not unexpectedly, the presence or lack of a bond critical point in the IAM density is also related to the kind of the adopted spherical atomic electron densities. In fact, rather than 8, only two of the 23 CH••O bond critical points found in the theoretical density are missing in the 6-21G promolecular density topology (Figure 6c).

(ii) The ρ_b values for the CH••O interactions that are described as bonded in both densities are spread in a much narrower range in the case of the IAM densities than are for the experimental densities (Figure 7c). The experimental trend of ρ_b vs $d_{H\cdot\cdot O}$ is much closer to the theoretical one than it is to that yielded by the IAM model. Conversely the $\nabla^2\rho_b$ trends for IAM and experimental densities (Figure 7b) are similar to each other and both show an exponential dependence on $d_{H\cdot\cdot O}$. Again, this close similarity refers only to those interactions that are found as bonded in both densities.

(iii) The trends in $G(\mathbf{r_b})$ and $V(\mathbf{r_b})$ for the experimental and IAM densities (Figure 7a) are very much alike, in agreement with the similar behavior observed for the $\nabla^2\rho_b$ values (Figure 7b) and the considerations given earlier as for the dominance of the contributions from these latter quantities to the $G(\mathbf{r_b})$ values beyond $d_{H\cdot\cdot O} = 2.5$ Å.

It appears that no significant information on $G(\mathbf{r_b})$ and $V(\mathbf{r_b})$ values at CH••O bond critical points is added by the experimental or theoretical crystal densities besides that already present in the corresponding promolecular densities. This conclusion holds in the range of $d_{H\cdot\cdot O}$ distances spanned by the *intermolecular* CH••O bonds in DMACB crystal and applies only to those interactions that are bonded both in the model and in the crystal density.

On the other hand, the promolecular model seems less capable to describe the "true" crystal density $\rho(\mathbf{r_b})$ at the BCP of these intermolecular interactions and, in some instances, to even recover the electron density topology (i.e. the BCP) that denotes their occurrence. This point is particularly important since, considering the theoretical electron densities only, we have observed[86] that the discrepancies between promolecular and "true" crystal densities are generally found to be at a minimum in the regions around the intermolecular critical points. As shown in Figure 8, this observation also holds true for the DMACB crystal. The density differences between promolecular and theoretical density (Figure 8a) are much larger (well) inside the atomic basins of the H and O atoms involved in the intermolecular interactions. Significant densities differences in the intermolecular regions that are not too close to the intermolecular BCPs or surfaces, also persist when the "true" crystal densities are compared to the procrystal densities (Figure 8b). The take-home message is that the signature of the formation of CH••O intermolecular interactions is much more in the charge rearrangements occurring inside the atomic basins—and, thus, in the changes of their atomic properties—rather than in the local changes in regions close to the intermolecular BCPs. This observation fits well with the significant charge rearrangements following H-bond formation which have been discussed in Section 3 and that are at the basis of the effectiveness of Koch and Popelier criteria to establish hydrogen bonds.

5. Conclusions

The present work has highlighted the potentialities of the electron density topological analysis for the study of the CH••O contacts in the DMACB crystal. This system represents an excellent candidate for studying the nature of CH••O interactions in solids. No other kind of stronger, and thus successfully competing hydrogen bond, is present in the crystal.

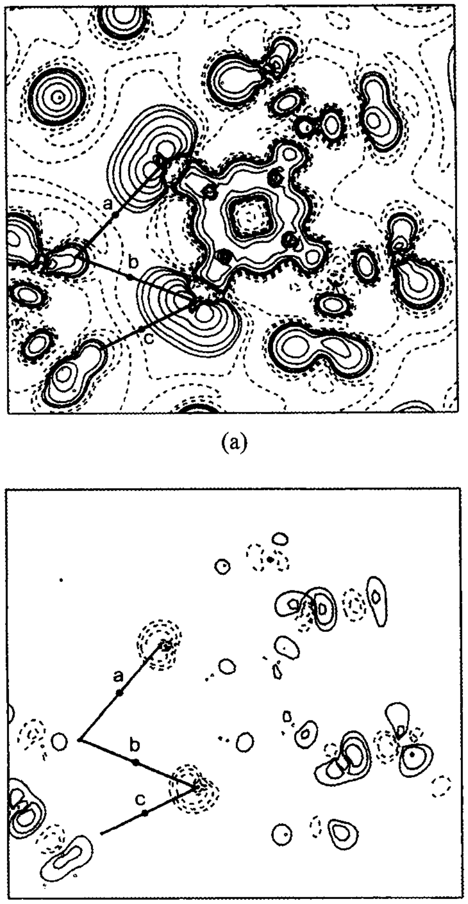

(a)

(b)

Figure 8. (a) Deformation (crystal − promolecular) and (b) interaction (crystal − procrystal) RHF/6-21G densities contour plots ($\pm a \times 10^{-n}$ au, $a = 2, 4, 8$; $n = 0-3$) in DMACB crystals. Bond paths from the hydrogen atoms to their acceptor oxygens (a, H53A−O2B, $d_{H\cdots O} =$ 2.453 Å; b, H53A−O1B, $d_{H\cdots O} = 2.907$ Å; c, H62A−O1B, $d_{H\cdots O} =$ 2.942 Å) are depicted as heavy lines and the associated bond critical points as dots.

Experimental densities obtained from single-crystal X-ray diffraction data and theoretical densities derived from periodic Hartree−Fock calculations have been topologically characterized and compared to each other. Using the bond path criterion, we have been able to discriminate between *bonded* and *nonbonded* CH••O contacts in DMACB, regardless of the value of their H•••O separation. The *bonded* contacts are characterized by a nearly constant and large C−H−O angle, denoting the importance of the electrostatic energy contribution to such interactions. Conversely the *nonbonded* contacts may be fold down to 90° since their dominant van der Waals contribution to the interaction energy is independent of the C−H−O angle. The almost isotropic CH••O angular distribution observed for H•••O separations greater than 2.7 Å is only apparent as it clearly disappears when the *bonded* and *nonbonded* contacts are identified and their angular distributions separately analyzed.

The Koch and Popelier criteria[15] to establish H-bonds have been applied for the first time in their wholeness to a large set of CH••O contacts in a crystalline phase. We found that each of these criteria was satisfied by all of the bonded intermolecular CH••O contacts, apart from a single exception concerning one long bond and one of the criteria only.

We have explored whether the expressions proposed by Espinosa et al.,[24,25] relating the potential energy densities $V(\mathbf{r_b})$ at the critical point to the H-bond strengths, also apply to the weak CH··O interactions in the DMACB crystal. We have shown that in the range of H···O separations investigated, the H-bond energies largely deviate from the $0.5V(\mathbf{r_b})$ value as found instead by Espinosa et al. at shorter distances and for the stronger XH··O (X = O, N) bonds. New expressions relating $V(\mathbf{r_b})$ to the H-bond energies are proposed in this work. They apply to the range $2.2 < d_{H\cdot\cdot O} < 3.0$ Å and yield energy estimates in very close agreement to those obtained by Espinosa et al. from a fit of theoretical H-bond dissociation energies vs $d_{H\cdot\cdot O}$. The estimated H-bond energies account for the total interaction energies of two representative DMACB dimers extracted from the crystal structure. On the other hand, the total interaction energy in the crystal is about twice of that estimated from the intermolecular H-bond formation energies, because of the large enhancement of the molecular dipole moment occurring upon crystallization. This greatly increases the electrostatic contribution from the molecular dipoles interactions.[21]

The importance of the promolecular charge distributions in defining topological properties of interest to the CH··O bonds was investigated. The criticism raised by Spackman[27] as to the lack of additional information provided by the experimental results to the description of such weak interactions was also addressed. We have shown that the promolecular density differs from the corresponding multipole or theoretical estimates as far as the electron density values at the critical point or, in some instances, even the density topology, is concerned. However, for those CH··O contacts that are identified as being *bonded* by both the promolecular and the crystal densities, the values of the kinetic or potential energy densities at the critical point obtained from either density are very much the same. The underlying reasons for such a property have been discussed.

We have also shown that the differences between promolecular and crystal densities are minimized close to the intermolecular surfaces or bond critical points, while the two densities may considerably differ (well) inside the atomic basins of the O and H atoms involved in the intermolecular interactions. This observation also applies when the procrystal density is compared to the crystal density, thereby accounting for the effectiveness of Koch and Popelier's criteria to establish H-bonds, even when the latter are rather weak and are formed upon crystallization.

Acknowledgment. This research was supported by the Italian MURST and CNR. We thank Mario Bandera for helping us in the preparation of the drawings.

References and Notes

(1) Jeffrey, G. A. *An Introduction to Hydrogen Bonding*; Oxford University Press: New York, 1997.

(2) Steiner, T. *Chem. Commun*. **1997**, 727 and references therein.

(3) Desiraju, G. R. *Acc. Chem. Res.* **1991**, *24*, 290.

(4) Jeffrey, G. A. *J. Mol. Struct. (THEOCHEM)* **1999**, *485−486*, 293.

(5) Donohue, J. In *Structural Chemistry and Molecular Biology*; Rich, A., Davidson, N., Eds.; Freeman: San Francisco, 1968; p 443.

(6) Green, R. D. *Hydrogen Bonding by C−H Groups*; MacMillan: London, 1974.

(7) Sutor, D. J. *J. Chem. Soc.* **1963**, 1105.

(8) Jeffrey, G. A.; Saenger, W. *Hydrogen Bonding in Biological Structures*; Springer: Berlin, 1991.

(9) Steiner, T.; Desiraju, G. R. *Chem. Commun*. **1998**, 891.

(10) Cotton, F. A.; Daniels, L. M.; Jordan, G. T., IV; Murillo, C. A. *Chem. Commun*. **1997**, 1673.

(11) Berkovitch-Yellin, Z.; Leiserowitz, L. *Acta Crystallogr.* **1984**, *B40*, 159.

(12) Mallinson, P. R.; Wozniak, K.; Smith, G. T.; McCormack, K. L. *J. Am. Chem. Soc.* **1997**, *119*, 11502.

(13) Platts, J. A.; Howard, S. T.; Wozniak, K. *Chem. Commun*. **1996**, 63.

(14) Cubero, E.; Orozco, M.; Hobza, P.; Luque, F. J. *J. Phys. Chem. A* **1999**, *103*, 6394.

(15) Koch, U.; Popelier, P. L. A. *J. Phys. Chem.* **1995**, *99*, 9747.

(16) Gu, Y.; Kar, Y.; Scheiner, S. *J. Am. Chem. Soc.* **1999**, *121*, 9411.

(17) CH donors with sp^3 hybridization show CH bond contraction and a blue shift in its vibrational frequency upon formation of the H-bond, while OH donors exhibit always a OH bond stretching and a frequency red shift following H-bond formation.

(18) Hobza, P.; Spirko, V.; Selzle, H. L.; Schlag, E. W. *J. Phys. Chem. A* **1998**, *102*, 2501.

(19) Hobza, P.; Havlas, Z. *Chem. Phys. Lett.* **1999**, *303*, 447.

(20) Müller-Dethlefs, K.; Hobza, P. *Chem. Rev.* **2000**, *100*, 143.

(21) May, E.; Destro, R.; Gatti, C. *J. Am. Chem. Soc.* **2001**, *123*, 12248.

(22) Coppens, P. *X-ray Charge Densities and Chemical Bonding*; IUCr Texts on Crystallography 4; Oxford Science Publications: New York, 1997.

(23) Lunelli, B.; Roversi, P.; Ortoleva, E.; Destro, R. *J. Chem. Soc., Faraday Trans.* **1996**, *92*, 3611.

(24) Espinosa, E.; Molins, E.; Lecomte, C. *Chem. Phys. Lett.* **1998**, *285*, 170.

(25) Espinosa, E.; Souhassou, M.; Lachekar, H.; Lecomte, C. *Acta Crystallogr*. **1999**, *B55*, 563.

(26) Espinosa, E.; Molins, E. *J. Chem. Phys.* **2000**, *113*, 5686.

(27) Spackman, M. A. *Chem. Phys. Lett.* **1999**, *301*, 425.

(28) Destro, R. *Chem. Phys. Lett.* **1997**, *275*, 463.

(29) Crystal data for the $P\bar{1}$(low T) phase: $C_8H_{12}N_2O_2$, $Z = 4$, $a = 6.7965(6)$, $b = 13.7743(15)$, $c = 8.7727(16)$ Å; $\alpha = 90.05(1)$, $\beta = 101.89(1)$, $\gamma = 91.96(2)°$.

(30) Steiner, T. *Cryst. Rev.* **1996**, *6*, 1.

(31) Destro, R.; May, E.; Gatti, C., in preparation.

(32) Stewart, R. F.; Bentley, J. J.; Goodman B. *J. Chem. Phys.* **1975**, *63*, 3786.

(33) Stewart, R. F.; Spackman, M. A. *VALRAY User's Manual*; Department of Chemistry, Carnegie-Mellon University, Pittsburgh, 1983.

(34) Allen, F. H.; Kennard, O.; Watson, D. G.; Brammer, L.; Orpen, A. G.; Taylor, R. In *International Tables for Crystallography*; Wilson, A. J. C. Ed.; Kluwer Academic Publishers: Dordrecht, 1995; Vol. C, p 696.

(35) Destro, R.; Roversi, P.; Barzaghi, M.; Marsh R. E. *J. Phys. Chem. A* **2000**, *104*, 1047.

(36) Schomaker, V.; Trueblood, K. N. *Acta Crystallogr. B* **1968**, *24*, 63.

(37) Saunders: V. R.; Dovesi, R.; Roetti, C.; Causà, M.; Harrison, N. M.; Orlando, R.; Zicovich-Wilson, C. M. *CRYSTAL98, User's Manual;* University of Torino: Torino, 1998.

(38) Hehre, W. J.; Radom, L.; Schleyer, P. v. R.; Pople, J. A. *Ab Initio Molecular Orbital Theory*; Wiley-Interscience: New York, 1986, and references therein.

(39) Elapsed CPU times for evaluating the atomic properties of one heavy atom in the DMACB crystal were typically as large as 40−50 h, using a RISC machine of about 10 SPECfp95 CPU peak performance.

(40) We tested unsuccessfully a number of procedures to facilitate the density matrix convergence in the SCF step. Namely (a) the initial guess of shell populations from a previous 6-21G computation; (b) the use of either the eigenvalue level shifting or the Fock matrix damping techniques.

(41) Spackman, M. A.; Mitchell, A. S. *Phys. Chem. Chem. Phys.* **2001**, *3*, 1518.

(42) The default value of the five parameters (ITOL1, ITOL2, ITOL3, ITOL4, ITOL5) that control the accuracy of calculation of bielectronic Coulomb and exchange series in CRYSTAL-98, are 6 6 6 6 12. We have used a more stringent set, 8 8 8 8 16, with ITOL5 minus ITOL4 equal to 8 as suggested by Spackman et al.

(43) Ditchfield, R.; Hehre, W. J.; Pople, J. A. *J. Chem. Phys.* **1971**, *54*, 724.

(44) Boys, S. F.; Bernardi, F. *Mol. Phys.* **1970**, *19*, 553.

(45) As reported by Spackman et al. (ref 41) for some prototypical molecular organic crystals, CPU times for basis sets with the $s = p$ constraint are as much as five times smaller than for a basis set of the same size and with no such a constraint.

(46) Bader, R. F. W. *Atoms in Molecules: A Quantum theory*; Int. Series of Monographs on Chemistry 22; Oxford University: Oxford, 1990.

(47) Tsirelson, V. G.; Zou, P. F.; Tang, T.-H.; Bader, R. F. W. *Acta Crystallogr*. **1995**, *A51*, 143.

(48) Bader, R. F. W.; Essen, H. *J. Chem. Phys.* **1984**, *80*, 1943.

(49) Gatti, C. *TOPOND-98: an electron density topological program for systems periodic in N (N = 0−3) dimensions*, User's Manual, CNR−CSRSRC, Milano, 1999.

(50) Barzaghi, M., personal communication.

(51) Keith, T. A. Ph.D. Thesis, McMaster University, 1993.

(52) PROAIMV, McMaster University, Ontario, Canada, 1992.

(53) Accuracy of the numerical determination of integrated properties was judged against the computed values for the atomic Lagrangian $L_\Omega = -1/4\int_\Omega \nabla^2\rho$, a quantity that should vanish because of the atomic basin boundary conditions. Obtained values of L_Ω were typically less than 10^{-4} and 10^{-3} au for hydrogen and the remaining atoms, respectively. The total

number of integrated electrons differs from the theoretical value by less than 0.009 au in all of the investigated systems.

(54) Bondi, A. *J. Phys. Chem.* **1964**, *68*, 441.

(55) Table 1 shows that experimentally no BCP is found also in the case of O2A−H51A and O1B−H72B contacts with α_{CHO} angles of 130.8 and 121.9°, respectively.

(56) Carroll, M. T.; Bader, R. F. W. *Mol. Phys.* **1988**, *65*, 695.

(57) Gatti, C.; Saunders, V. R.; Roetti, C. *J. Chem. Phys.* **1994**, *101*, 10686.

(58) For conventional hydrogen bonds with hydroxy donors the O−H··Y angle is 154.0(4)° (see ref 8).

(59) Destro, R.; Merati, F. *Acta Crystallogr.* **1995**, *B51*, 559.

(60) Pichon-Pesme, V.; Lecomte, C. *Acta Crystallogr.* **1998**, *B54*, 485 and ref 25.

(61) Bianchi, R.; Gatti, C.; Adovasio, V.; Nardelli, M. *Acta Crystallogr.* **1996**, *B52*, 471.

(62) Popelier, P. L. A. *J. Phys. Chem. A* **1998**, *102*, 1873.

(63) Jenkins, S.; Morrison, I. *J. Phys. Chem. B* **1999**, *103*, 11041.

(64) The bonded radius of X is the distance from the nucleus X to the H-bond critical point, while the nonbonded radius of X was calculated as the distance of its nucleus to the 0.001 au contour in the isolated molecule. This latter distance is measured in the direction of H-bond formation as seen from the nucleus. The 0.001 au contour was adopted as this electron density envelope yields (ref 46) molecular sizes and atomic diameters in good agreement with gas-phase van der Waals' radii.

(65) It is worth noting that the reported increases of the H83A and H83B volumes and the small energy stabilization of H63B atom are within the estimated "error bars" of the atomic integration (ref 66).

(66) Aicken, F. M.; Popelier, P. L. A. *Can. J. Chem.* **2000**, *78*, 415.

(67) On the basis of the established link (ref 56) between the softness of an acid and the increased penetration of its hydrogen by the base atom B (B═O, here), Koch and Popelier suggested that the CH group should be considered as a soft acidic group. However they noticed that "it would be interesting to collect further support for this observation from elsewhere". Our data clearly strengthen this earlier finding, because of the large number of CH··O bonds present in the DMACB crystal, the wide range of H-bond distances they span and the very large $\Delta r(H)/\Delta r(O)$ ratios found. These latter were calculated to be about 2 for the shortest and as large as 40−50 for the longest H-bonds in the DMACB crystal, while they never exceeded the value of 1.6 in the anti-AIDS compound. This result gives further evidence to considering the CH acidic group as a soft one, a conclusion put forth also by Desiraju (ref 68) using a crystal engineering approach. The larger H-atom penetrations found in DMACB, rather than be a real indication of the CH acidic group softness, could be just the result of the concurrent decreased capability of the O acceptors of being penetrated, because of their involvement in so many H-bond interactions in the crystal. However, previous results on the urea crystal (ref 57), where the O atoms are each involved in four NH···O interactions and where the $\Delta r(H)/\Delta r(O)$ ratios never exceeded 1.3, seem to exclude the dominance of such an effect in yielding very high $\Delta r(H)/\Delta r(O)$ ratios in the DMACB crystal.

(68) Desiraju, G. R. *Angew. Chem., Int. Ed. Engl.* **1995**, *34*, 2311.

(69) The small dipolar polarization decrease of H atoms is opposite to the trend exhibited by the other quantities. This apparently different behavior may be easily explained. Indeed, crystallization is generally (ref 57) accompanied by a reduction in the atomic polarization and the formation of an H-bond in the bulk reinforces such a decrease. This is clearly evident from the noticeable decreases (about 0.2−0.3 au) of dipolar polarization found for the H atoms involved in the intermolecular CH···O interactions. Instead, in the case of the intramolecular ones, the decrease of dipolar polarization induced by crystallization is counterbalanced by the increase of $\mu(H)$ which is caused by the diminished loss of the nonbonded density of the hydrogen atoms in the bulk (compare r(H) and N(H) vs $r^0(H)$ and $N^0(H)$). The net result is just a negligible decrease of $\mu(H)$ in the bulk.

(70) For the H53A hydrogen atom, which is involved in a bifurcated intercolumn H-bond, $\Delta N(H)$ is proportionally apportioned between the two bonds it forms, according to the inverse of their H-bond distance.

(71) The use of optimized geometries for both the gas phase and the bulk would certainly facilitate the exploration of the usefulness of the "*differential*" Koch and Popelier's criteria. However this further study is out of the scope of the present paper.

(72) Spackman, M. A. *J. Phys. Chem.* **1987**, *91*, 3179.

(73) Spackman, M. A.; Weber, H. P.; Craven, B. M. *J. Am. Chem. Soc.* **1988**, *110*, 775.

(74) Coppens, P.; Abramov, Y. A.; Carducci, M.; Korjov, B.; Novozhilova, I.; Alhambra, C.; Pressprich, M. R. *J. Am. Chem. Soc.* **1999**, *121*, 2585.

(75) Abramov, Y. A.; Volkov, A.; Wu, G.; Coppens, P. *J. Phys. Chem. B* **2000**, *104*, 2183.

(76) Abramov, Y. A.; Volkov, A.; Coppens, P. *J. Mol. Struct.* (*THEOCHEM*) **2000**, *529*, 27.

(77) Abramov, Y. A.; Volkov, A.; Wu, G.; Coppens, P. *Acta Crystallogr. A* **2000**, *56*, 585.

(78) For the selection of the ghost atoms we adopted a distance cutoff of 3.5 Å from any of the atoms forming the molecule. In the case of the dimers, the full counterpoise procedure was used.

(79) Abramov, Y. A. *Acta Crystallogr.* **1997**, *A53*, 264.

(80) The use of this relationship to derive $V(\mathbf{r_b})$ from experimental $G(\mathbf{r_b})$ data assumes that the multipolar-derived electron distribution obeys the local virial theorem, while it actually does not.

(81) In ref 26, Espinosa and Molins retrieve an expression for the H···O interaction potential $U(\mathbf{r})$ by combining their empirical formula [24] relating the potential and kinetic energy density at the BCP (and hence also their sum, the local energy density) to the H··O separation with the experimental force constant of the H-bonds in ice VIII. The so obtained $U(\mathbf{r})$ expression represents a new interaction H··O potential directly derived from the topological analysis of the electron density distribution. However, since the use of such a potential to evaluate the H-bond energies would require the knowledge of the polarization energy, U_{pol}, at each point r of the interaction curve and not only at its minimum r_0, we could not test also this new proposed expression in our analysis.

(82) For the sake of comparison with both the experiment and the Espinosa et al. relationships, we used the $V(\mathbf{r_b})$ data obtained through Abramov's approach also in the case of theoretical densities.

(83) In the case of the experimental $V(\mathbf{r_b})$ data set, the datum at $d_{H\cdot\cdot O} =$ 2.570 Å was omitted from the fit because visibly out of range.

(84) The same energy contribution would be obviously obtained by summing half of the energy—to avoid double counting—of the intermolecular H-bonds formed by molecules A and B. There are (Figure 2) 19 of such bonds involving molecule A (twelve bonds with the two adjacent A molecules within the column, 5 with B molecules in neighboring columns and two with A molecules related by translation along the *c*-axis) and 19 involving molecule B (12 bonds with the two adjacent B molecules within the column, 5 with A molecules in neighboring columns and two with B molecules related by translation along the *c*-axis).

(85) This observation is based on the Abramov's expression for $G(\mathbf{r})$. However, since this relationship approximates the exact $G(\mathbf{r})$ values remarkably well (see Table 5), the relative contributions of $\nabla^2\rho_b$ and ρ_b should similarly affect also the exact $G(\mathbf{r})$ values over the entire range of $d_{H\cdot\cdot O}$ considered.

(86) Gatti, C. Unpublished.